JAERI-Research
2002-010

NUCLEAR REACTIONS IN ULTRA-MAGNETIZED SUPERNOVAE

June 2002

V.N. Kondratyev*

日本原子力研究所
Japan Atomic Energy Research Institute

本レポートは、日本原子力研究所が不定期に公刊している研究報告書です。
入手の問合わせは、日本原子力研究所研究情報部研究情報課（〒319-1195　茨城県那珂郡東海村）あて、お申し越し下さい。なお、このほかに財団法人原子力弘済会資料センター（〒319-1195　茨城県那珂郡東海村日本原子力研究所内）で複写による実費頒布を行っております。

This report is issued irregularly.
Inquiries about availability of the reports should be addressed to Research Information Division, Department of Intellectual Resources, Japan Atomic Energy Research Institute, Tokai-mura, Naka-gun, Ibaraki-ken 〒319-1195, Japan.

編集兼発行　日本原子力研究所

JAERI－Research 2002－010

Nuclear Reactions in Ultra-magnetized Supernovae

V.N. Kondratyev*

Advanced Science Research Center
(Tokai Site)
Japan Atomic Energy Research Institute
Tokai-mura, Naka-gun, Ibaraki-ken

(Received April 1, 2002)

The statistical model is employed to investigate nuclear reactions in ultrastrong magnetic fields relevant for supernovae and neutron stars. For radiative capture processes the predominant mechanisms are argued to correspond to modifications of nuclear level densities, and γ-transition energies due to interactions of the field with magnetic moments of nuclei. The density of states reflects the nuclear structure and results in oscillations of reaction cross sections as a function of field strength, while magnetic interaction energy enhances radiative neutron capture process. Implications in the synthesis of r-process nuclei in supernova site are discussed.

PACS: 26.30.+k, 26.50.+x, 25.40.Lw, 98.38. Mz

Keywords: Neutron Capture Reaction, Nucleosynthesis, Nuclear Shell Effect, Supernova, Magnetic Field

---

* Kiev Institute for Nuclear Research
(JAERI Research Fellow : Mar.1,1999 ～ Feb.28, 2002)

超強磁場超新星中の核反応

日本原子力研究所先端基礎研究センター
V.N. Kondratyev*（コンドラチェフ　ヴォロディミール）

（２００２年４月１日受理）

超新星や中性子星における超強磁場中での核反応を統計模型をもとに検討した。γ線放出を伴う中性子捕獲過程については、磁場による準位密度の変化とγ遷移エネルギーの変化が主要なメカニズムとして効くことが分かった。すなわち、核構造を反映する準位密度が磁場強度の変化による変動を示すことに伴って反応断面積の変動があらわれ、また磁場による相互作用エネルギーが中性子捕獲過程を増大させる。さらに、超新星コアにおけるｒ-プロセス核の生成について検討した。

日本原子力研究所（東海駐在）：〒319-1195　茨城県那珂郡東海村白方白根 2-4
*キエフ原子核研究所（原研リサーチフェロー：1999 年 3 月 1 日～2002 年 2 月 28 日）

Contents

目　　次

1. Introduction: Amplified Magnetic Fields in Supernova Core and Neutron Star

The supernova (SN) is long considered as promising astrophysical site candidate for r-process nuclei (see, e.g., Fowler, Caughlan & Zimmerman 1967, 1975, Fowler 1984, Rolfs & Rodney 1988). The capture reactions play an important role in respective nucleosynthesis studies which usually exploit nuclear data corresponding to laboratory conditions (see Fowler, Caughlan & Zimmerman 1975, Fowler 1984, Rolfs & Rodney 1988, Meyer & Brown 1997, Hoffman et al. 1999 and refs. therein). The astrophysical environment can, however, affect significantly the cross sections of key nuclear reactions. In particular, ultrastrong magnetic fields can develop in the core of Type II or Ibc supernovas (Duncan & Thompson 1992). Recent analysis (cf., e.g., Thompson 2000, Thompson & Murray 2001) of field amplification process due to violent convective motion indicates that inside the neutrino-sphere (of a radius of 30 km) the root-mean-square field strength can exceed $10^{15.5}$ G, while in vicinity of rapidly rotating nascent neutron stars the strength can range up to $B \sim 10^{18}$ G. During past decade the observations of soft gamma repeaters (SGRs) and anomalous X-ray pulsars (AXPs) brought numerous evidences in support of such a 'magnetar' concept asserting thereby a possibility of such enormous stellar magnetic fields. The supporting evidences appear as, e.g., short bright outbursts (Mazets et al. 1979, Hurley et al. 1999, Feroci et al. 2001) and optical data (Kaplan 2001) for SGRs, rapid braking of relatively slowly rotating stars identified with SGRs (Kouveliotou et al. 1998, Kouveliotou et al. 1999) and AXPs (Gotthelf, Vasisht & Dotani 1999, Kaspi, Chakrabarty & Steinberger 1999). These pulsars are associated with SN remnants (see, e.g., Feroci et al. 2001 and refs. therein).

The field strengths relevant to 'magnetars' correspond to a flux $\Phi_0 \sim \hbar c/\pi e$ through an area covered by the size of nuclei. As pointed out recently by Kondratyev et al. (1999, 2000, 2001, 2002) such magnetic fields can dramatically modify the structure of nuclei and, consequently, influence nuclear reactions (Kondratyev 2002a). Incorporating magnetic field effects in an analysis of nuclear reaction network might provide more insights on supernova explosion and, in particular, magnetodynamics in supernova core.

In sect. 2 we outline basic concepts for the description of nuclear reaction rates in ultra-magnetized stellar media. The statistical model is applied in sect. 3 to study nuclear reactions in magnetic fields. As demonstrated for radiative capture process apart from the change in the nuclear structure considerable mechanism is represented by the modification of gamma-transition energy due to the interaction of the field with magnetic moments of reaction partners. Such a change of the energy is shown in sect. 4 to result in an enhancement of high spin-states population. The systematic investigation nuclear structure in magnetic fields is given in sect. 5. Possible influence of strong magnetization of stellar matter on r-process paths is discussed in sect. 6. The conclusions are in sect. 7.

2. Thermonuclear Reaction Rates in Magnetic Fields

The reaction rates r are defined as the number of reactions per unit of volume and time, e.g., cm^3 and sec, between nuclear particles, say target I and projectile i. This quantity can be expressed in terms of respective cross section σ and differential number densities $d\mathcal{D}_i$ and $d\mathcal{D}_I$ as

$$r_{I,i} = \int \sigma v_{iI} d\mathcal{D}_i d\mathcal{D}_I \,, \tag{1}$$

where $v_{iI} = |\mathbf{v}_i - \mathbf{v}_I|$, and vectors $\mathbf{v}_i$ and $\mathbf{v}_I$ denote the velocities of related nuclear components.

The evaluation of an integral in the right hand side of Eq. (1) depends on the type of involved particles and distributions. For magnetic fields of interest the nuclear particles in an astrophysical plasma can be described within non-relativistic treatment (Kondratyev 2001, 2001a). Furthermore, for relatively heavy nuclei we neglect an effect of Landau quantization. Then as in the case of neutron densities the distributions $d\mathcal{D}_i$ are expected to obey the Maxwell-Boltzmann function weighted with a factor determined by the projection of magnetic moments on the field axis $\mathcal{M}_I$

$$d\mathcal{D}_I = \mathcal{D}_I G_I^{-1} \exp\{-(E_\nu + \mathcal{M}_I B)/k_\mathrm{B}T\} \left(\frac{m_I}{2\pi kT}\right)^{3/2} \exp\{-m_I v_I^2/2k_\mathrm{B}T\} d^3 v_i \tag{2}$$

with spatial density $\mathcal{D}_i$. The partition function

$$G_I = \sum_\nu \exp\{-(E_\nu + \mathcal{M}_I B)/k_\mathrm{B}T\} \tag{3}$$

is determined by excitation spectrum E_ν, and the Boltzmann constant k_B.

For neutrons, $I \equiv \mathrm{n}$, two possible spin projections $m_\mathrm{n} = \pm 1/2$ yield

$$G_\mathrm{n} = 2\cosh(g_\mathrm{n}\mu_\mathrm{N} B/2k_\mathrm{B}T) \,, \tag{4}$$

where the nucleon magneton $\mu_\mathrm{N} = e\hbar/2m_\mathrm{p}c \approx 3.15 \cdot 10^{-18}$ MeV·G^{-1} and the neutron g-factor $g_\mathrm{n} \approx -3.8263$. As seen for realistic temperatures $T \sim 10^9$ K and magnetic fields of a strength B exceeding 10^{15} G the distribution Eq. (2) is dominated by components with nuclear spins aligned along the field direction. Neglecting contributions of other projections on the field axis thermonuclear reaction rates are reduced to the well known (cf., e.g., Fowler, Caughlan & Zimmerman 1975) form

$$r_{I,i} = \langle \sigma v \rangle_{I,i} \mathcal{D}_i \mathcal{D}_I \tag{5}$$

$$\langle \sigma v \rangle_{I,i} = \left(\frac{8}{\mu_\mathrm{r}\pi}\right)^{1/2} (k_\mathrm{B}T)^{-3/2} \int_0^\infty E\sigma(E) \exp\{-E/k_\mathrm{B}T\} dE \,. \tag{6}$$

Here μ_r denotes the reduced mass of the target-projectile system. To the best of our knowledge the laboratory experimental information on nuclear scattering in such super-strong magnetic fields is not available. The theoretical treatment based on statistical

description of compound nuclei has been widely used in astrophysical applications. It is, therefore, worthy to perform at initial steps an analysis of magnetic field effect in nuclear reactions on that level of approximation.

3. Statistical Description of Compound Nuclear Reactions

The Hauser-Feshbach statistical approach constitues useful framework for theoretical prediction of nuclear reaction cross sections for the vast number of medium and heavy nuclei which exhibit relatively high density of excited states already at neutron capture energies. At appropriate excitation energies such small level spacing in the compound nucleus allows to make use of the statistical model calculations for compound nuclear reactions (see, e.g., Hauser & Feshbach 1952, Mahaux & Weidenmüller 1979, Feshbach 1992) with strongly overlapping resonances. The applicability of such a treatment for astrophysics has been extensively discussed recently, e.g., by Rauscher, Thielemann & Kratz 1997. The only necessary condition for its application is a large number of resonances at the appropriate relative velocities v_{iI}, so that the cross section can be described by an average over resonances. This can in specific cases be valid also for light nuclei, while on the other hand not be valid for intermediate mass nuclei in vicinity of magic numbers. In the most practical cases the statistical model yields highly accurate cross sections, when the required ingredients are sufficiently reliable. Analysis of the magnetic field dependence of respective inputs provides, therefore, an information on the field effect in the reaction rates.

3.1. Theoretical Predictions of Reaction Cross Sections

Within the statistical theory the nuclear reaction cross sections are expressed in terms of averaged transmission coefficients T, which do not reflect resonance features, but rather describe the absorption via an imaginary part in the (optical) nucleon-nucleus potential (Mahaux & Weidenmüller 1979). The high level density in the compound nucleus allows to employ such an average treatment which leads to the well known expression

$$\sigma_I^{\mu\nu}(i,o;E_{iI}) = \pi\lambda^2 \sum_{m,\pi} \frac{T_i^{\mu}(E,m,\pi,E_I^{\mu},m_I^{\mu},\pi_I^{\mu}) T_o^{\nu}(E,m,\pi,E_O^{\nu},m_O^{\nu},\pi_O^{\nu})}{T_{tot}(E,m,\pi)} \qquad (7)$$

for the reaction $I^{\mu}(i,o)O^{\nu}$ from the target state I^{μ} to the exited state O^{ν} of the final nucleus, with the wave-length $\lambda = \hbar/\mu_r v_{nI}$, m denotes the projection of spin, E the corresponding excitation energy in the compound nucleus, and π the parity of excited states. When these properties are used without subscripts they describe the compound nucleus, while subscripts refer to states of the participating nuclei in the reaction $I^{\mu}(i,o)O^{\nu}$ and superscripts indicate the specific excited states. We note that experimental measurements yield usually the data accumulating all excited states of the final nucleus, $\sum_{\nu} \sigma_I^{0\nu}(i,o;E_{iI})$,

with the target in the ground state. Since in an astrophysical plasma target states μ are thermally populated, the astrophysical cross section $\sigma_I^*(i,o)$ is given by

$$\sigma_I^*(i,o;E_{iI}) = G_I^{-1}\sum_\mu \exp\{-(E_I^\mu + \mathcal{M}_I B)/k_\mathrm{B}T\}\sum_\nu \sigma_I^{\mu\nu}(i,o;E_{iI}) \quad , \tag{8}$$

where the partition function is defined by Eq. (3).

The summation over ν replaces $T_o^\nu(E,m,\pi)$ in Eq. (7) by the total transmission coefficient

$$T_o(E,m,\pi) = \int_{-\infty}^{E-S_{O,o}} \sum_{J_O,\pi_O} T_o(E,m,\pi,E_O,m_O,\pi_O)\mathcal{W}(E_O,m_O,\pi_O)dE_O \quad , \tag{9}$$

where the upper integration limit is determined by the channel separation energy $S_{O,o}$, and the level density

$$\mathcal{W}(E_O,m_O,\pi_O) = \sum_\nu \delta(E_O - E_O(m_O^\nu,\pi_O)) \tag{10}$$

includes the summation over nuclear states ν corresponding to projection m_O^ν of a spin J_O^ν. The summation over target states μ in Eq. (8) is generalized accordingly by Holmes et al. 1976. It is important to stress here that the sensitivity of nuclear reactions in magnetic fields to projection of spins on the field axis requires to employ the spin-projection representation in Eq. (7). Such a sensitivity removes, in addition, the spin-degeneracy factors.

As indicated in Eqs. (7), (8) and (9) important ingredients of statistical model calculations are represented by the particle and gamma-transmission coefficients T, and level densities of excited states $\mathcal{W}$. Therefore, the effect of magnetic field in these components determines the field dependence of cross sections. As demonstrated by Kondratyev et al. (1999,2000,2001,2002) the non-relativistic mean-field treatment provides an accurate description of nuclei in magnetic fields of interest. Relativistic effects become important at considerably larger field strengths when the energy of the first Landau level $\omega_\mathrm{L} = \mu_\mathrm{N} B$ (with the nuclear magneton μ_N) becomes comparable to the nucleon rest mass. The magnitude of the respective limiting field for nucleons $B_\mathrm{rel}^\mathrm{N} = m_\mathrm{p}c^2/2\mu_\mathrm{N} \approx 1.5 \cdot 10^{20}$ G corresponds to a flux $\Phi_0 = \hbar c/\pi e$ through the area of a radius given by the nucleon Compton wavelength $\lambda_\mathrm{N} = \hbar/(m_\mathrm{p}c) \approx 0.21$ fm. These fields may affect, e.g., conditions of β-equilibrium of the neutron star bulk matter (Broderick, Prakash & Lattimer 2000). In sects. 3.2 and 3.3 we make use of this approach to analyze the constituents of statistical model.

3.2. Level Densities of Nuclei in Strong Magnetic Fields

The mean-field treatment brings the non-interacting Fermi-gas model (Bethe 1936, Bloch 1954, Feshbach 1992) for the nuclear level density. Most statistical model cal-

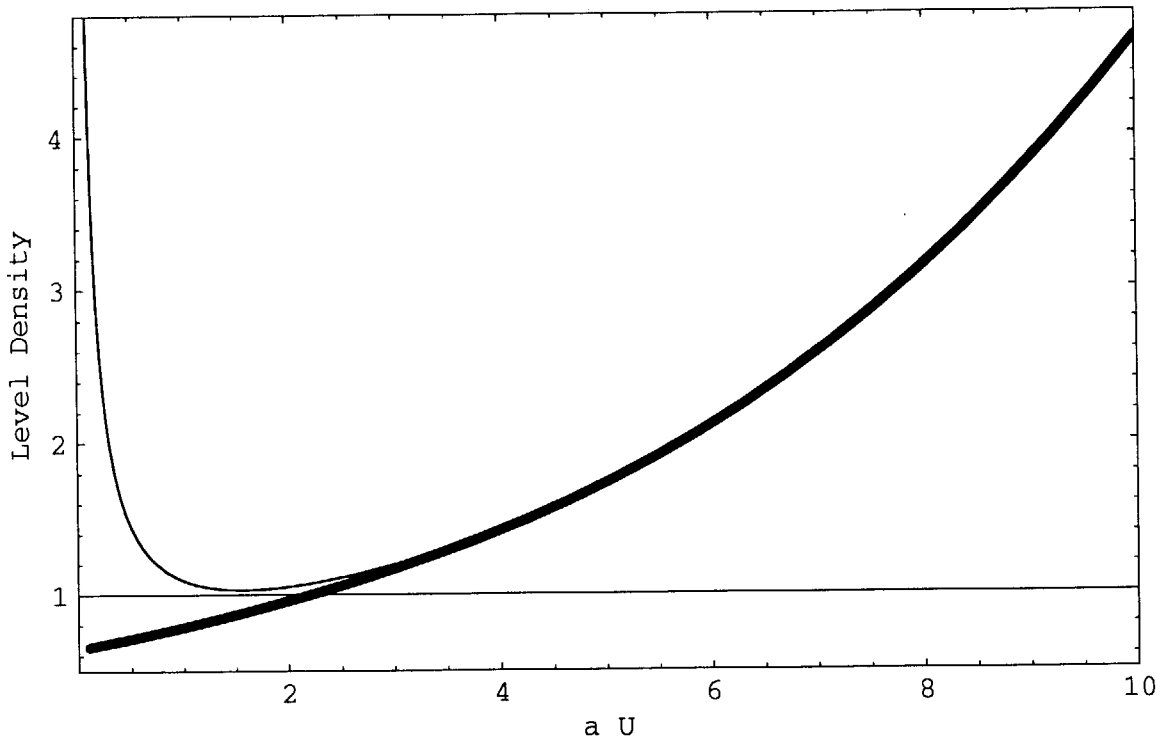

Fig. 1.— Level density in the units of $1/a$. Thin line shows Eq. (12), while thick solid line displays the behavior of regularized with constant temperature approximation Eq. (18) density of states.

culations use the back-shifted Fermi-gas description of Gilbert & Cameron (1965). More sophisticated Monte Carlo shell model calculations (e.g., Nakada & Alhassid 1997), as well as combinatorial approaches (see, e.g., Zuker 2001) show excellent agreement with the mean-field based approach and justify an applicability of the Fermi-gas description at and above the neutron separation energies. The phenomenological parameterization of density of states is given by

$$\mathcal{W}(U,m,\pi) = \frac{1}{2}\mathcal{F}(U,m)\mathcal{W}(U), \tag{11}$$

with excitation energy E dependent factor

$$\mathcal{W}(U) = \frac{\sqrt{\pi}}{12a^{1/4}}\frac{\exp(2\sqrt{aU})}{U^{5/4}}, \qquad U = E - \delta \tag{12}$$

which is defined by the level density parameter a and the back-shift δ providing a measure for an energy of the first excited state. The spin-projection dependence $\mathcal{F}$ is given by the Gaussian factor (Bloch 1954, Feshbach 1992)

$$\mathcal{F}(m) = (\sqrt{\pi}\kappa)^{-1}\exp\left(-(m-m_{\rm F})^2/\kappa^2\right) \tag{13}$$

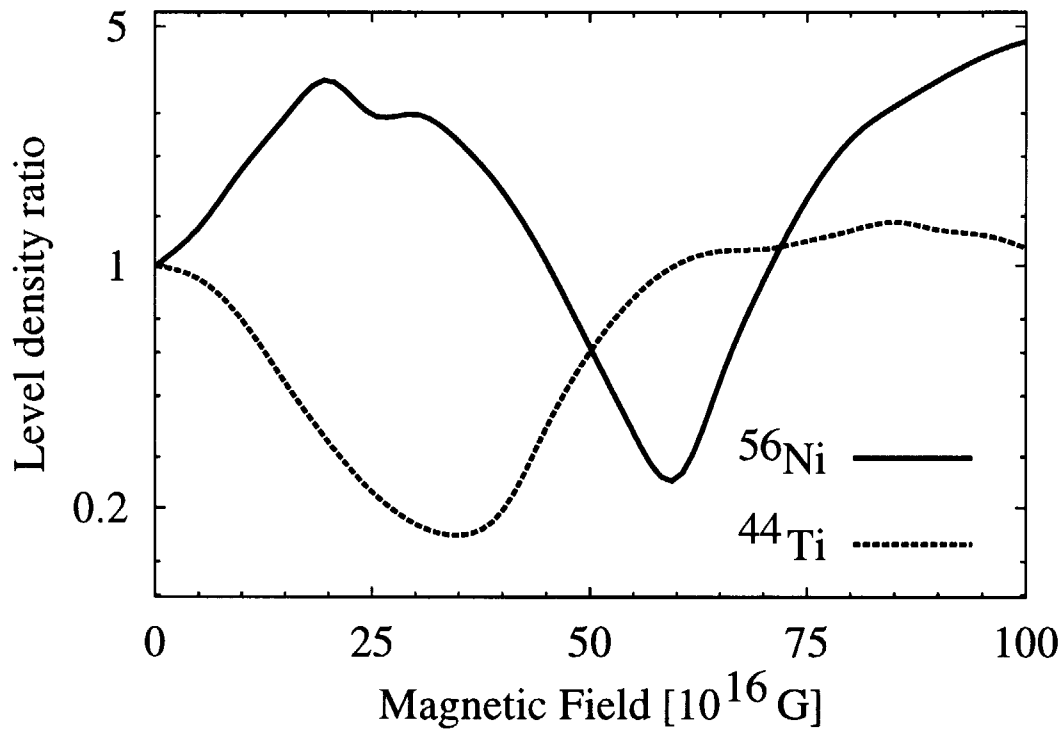

Fig. 2.— Magnetic field dependence of normalized at zero field nuclear level density at neutron separation energy for ^{56}Ni (solid line) and ^{44}Ti (dashed line).

centered at the projection $m_{\rm F}$ associated with the Fermi energy. The spin cut-off parameter is evaluated under an assumption of spherical rigid nucleus

$$\kappa^2 = \frac{\mathcal{J}_{\rm rigid}}{\hbar^2}\sqrt{\frac{U}{a}} \tag{14}$$

with the moment of inertia $\mathcal{J}_{\rm rigid} = (2/5)m_{\rm N}AR^2$.

Making use of the excitation-energy dependent description initially proposed by Ignatyuk et al. (1975) the level density parameter a is expressed by

$$a(U,Z,N) = \tilde{a}(A)[1 + C(Z,N)f(U)/U] \tag{15}$$

$$\tilde{a}(A) = \alpha A + \beta A^{2/3} \tag{16}$$

$$f(U) = 1 - \exp(-\gamma U). \tag{17}$$

The values of free parameters α, β and γ are determined by fitting to experimental level density data to yield (Rauscher, Thielemann & Kratz 1997) $\{\alpha, \beta, \gamma\}$ = {0.1337, -0.06571, 0.04884}.

The function $f(U)$ permits two extreme limits:

i– For small excitation energies Eq. (15) is reduced to the form proposed by Gilbert & Cameron (1965), $a/A = \alpha + \alpha\gamma C(Z,N)$. The value $C(Z,N)$ is identified with shell correction energy which is negative for magic nuclei.

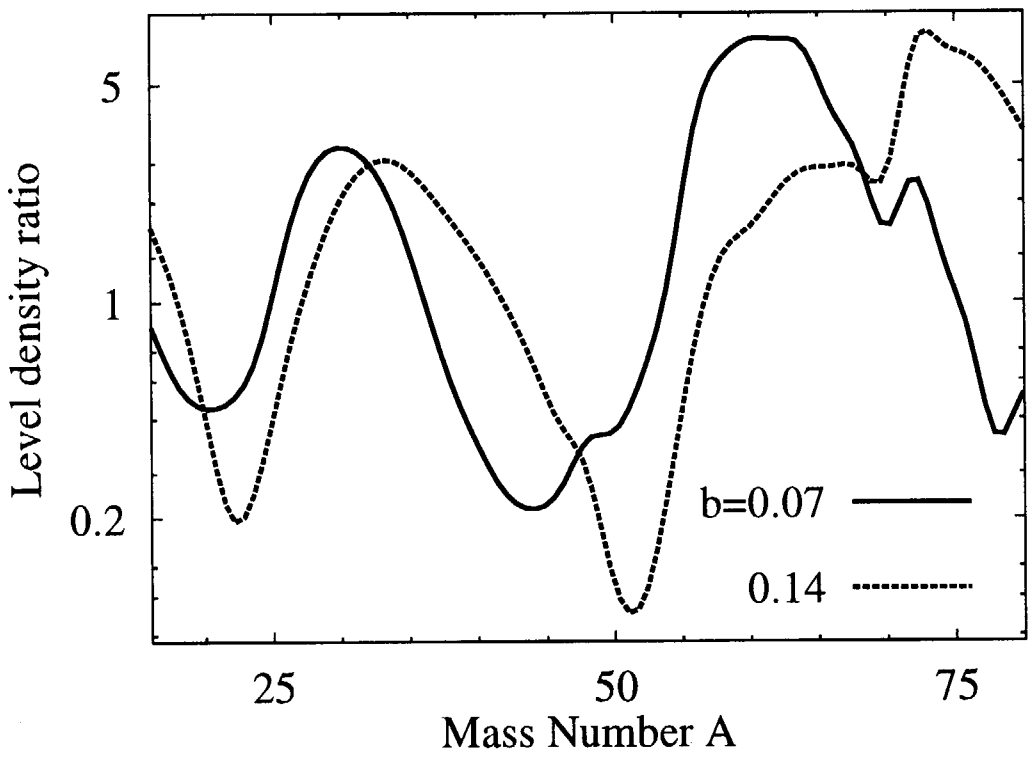

Fig. 3.— Normalized at zero field nuclear level density at neutron separation energy versus mass number at magnetic fields corresponding to values of parameter $b = 0.07$ (solid line) and 0.14 (dashed line) which measures the field strength in the units ω_0/μ_N, see Eq. (19) and discussion therein.

ii– At high excitation energies the quantity of a/A approaches the continuum value α, obtained for infinite nuclear matter, accounting, thereby, for washing out shell effects.

At low energies $aU < 5$ we combine Eq. (12) with the constant temperature expression due to Gilbert & Cameron (1965)

$$\mathcal{W}(U) \propto \exp\{U/\tau\}/\tau \tag{18}$$

obtaining the value of τ from proper tangential behavior. Figure 1 illustrates that such a combination provides proper description of density of states at small energies, consistent with experimental results, as well as Monte Carlo shell model calculations (Nakada & Alhassid 1997) and combinatorial approaches (see, e.g., Zuker 2001).

As demonstrated by Kondratyev et al. (1999, 2000, 2001, 2002) the shell corrections dominate magnetic field effects in nuclear structure. Therefore in calculations of the level density we incorporate the magnetic field dependence through the shell correction part of the level density parameter, i.e. field dependent shell energy C_B in Eq. (15), while other quantities are considered as field independent. Then, normalized at zero field density of states can be expressed as

$$\frac{\mathcal{W}_B}{\mathcal{W}_0} \approx \exp\{2(\sqrt{a_B U} - \sqrt{a_0 U})\} \tag{19}$$

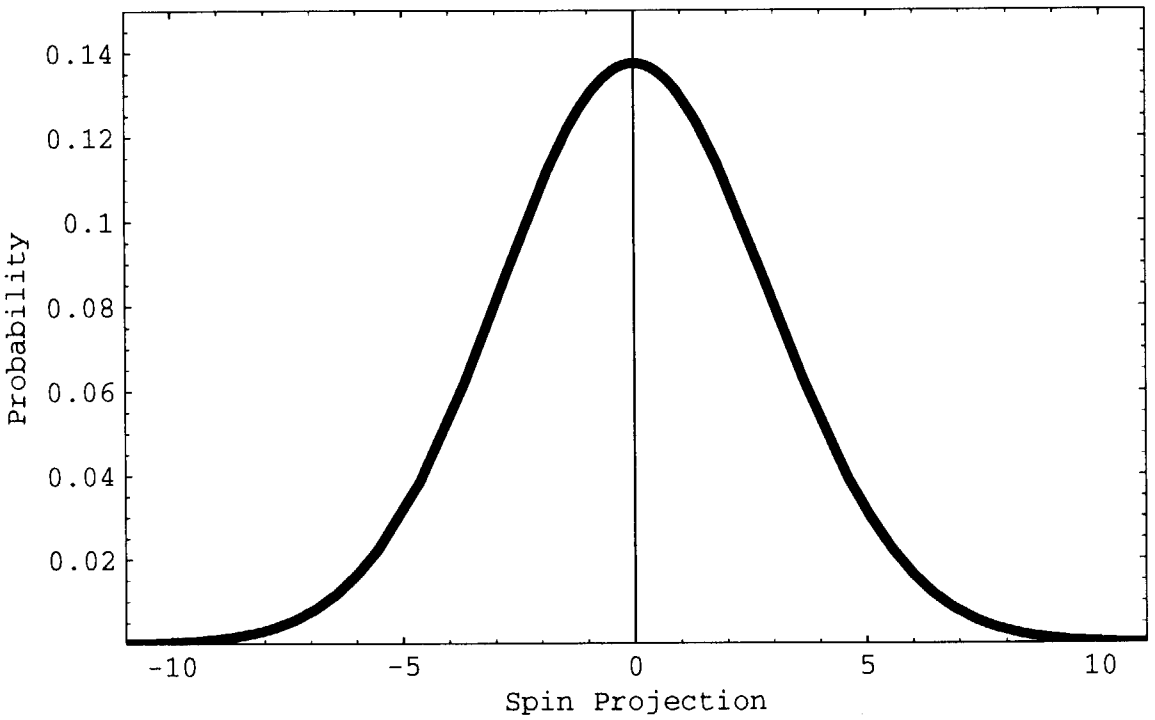

Fig. 4.— Distribution of spin-projection $(m - m_{\rm F})$, Eq. (13), for ^{56}Ni.

$$\approx \exp\{(C_B - C_0) f(U) \sqrt{\tilde{a}/U}\} \ . \tag{20}$$

In the latest evaluation we take into account the inequality $\gamma \ll 1$, see Eq. (15) and discussion therein. The magnetic field dependence of the shell energy is calculated and analyzed in sect. 5 (see also Kondratyev, Maruyama & Chiba 2000, Kondratyev 2001a). Making use of the results of the Nilsson model (NM) for spherical nuclei and Eq. (19) we consider the level density of nuclei in magnetic fields at neutron separation energies. As evident from fig. 2 the density of states oscillates as a function of magnetic field. The double magic ^{56}Ni in the laboratory displays increasing number of levels at weak fields, while the level spacing grows in case of slightly antimagic ^{44}Ti. Such a feature reflects the magic-antimagic switching (see sect. 5 and Kondratyev, Maruyama & Chiba 2000, Kondratyev 2001a) in nuclear structure at varying fields. Such a behavior is illustrated in more details in fig. 3 which shows mass number dependence of normalized density of states at various values $b = \mu_{\rm N} B/\omega_0$, where the NM parameter $\omega_0 \approx 41 A^{-1/3}$ MeV is associated with the energy difference between major shells. We see that the normalized at zero field level density oscillates as a function of mass number as well. The varying magnetic field induces a phase shift in mass number oscillations in normalized density of states.

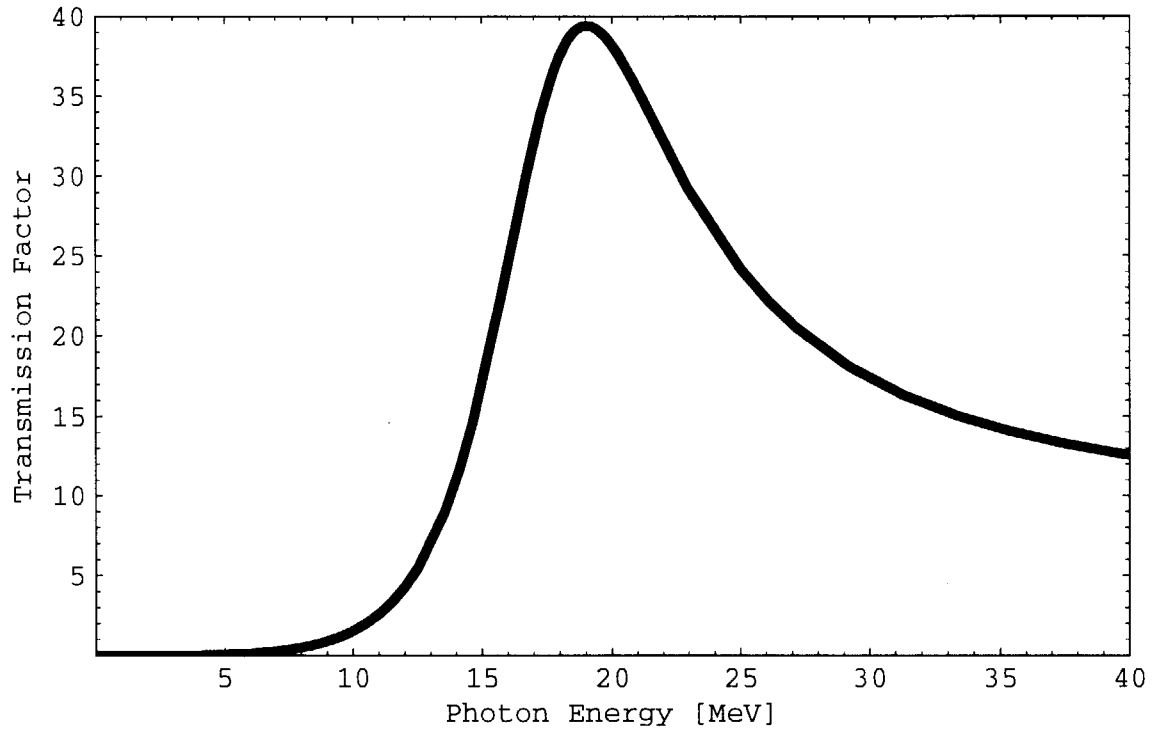

Fig. 5.— Energy dependence of ^{56}Ni E1-transmission factor in the units of $(8/3)\cdot(NZ/A)\cdot(e^2/\hbar m_{\rm N}c^3)$.

Assuming the radius $R \approx 1.25A^{1/3}$ fm and applying the leading term of Eq. (15) for the parameter a the value of spin cut-off is evaluated in an unified form to be $\kappa^2 \approx 0.225A^{2/3}\sqrt{aU}$. As illustrated in fig. 4 the nuclei of middle masses display wide spin distribution of densities of states as compared to change of spin projection given by selection rules for photon emission, see sect. 3.3.

3.3. Transmission Coefficients

The individual transmission coefficients in Eq. (9) provide a measure for transition rates from certain excited state in the compound nucleus (E, m, π) to the state $(E_I^\mu, m_I^\mu, \pi_I^\mu)$ in nucleus I via the emission of a particle i. Such a quantity can be expressed in terms of a summation over quantum mechanically allowed partial waves. We note, however, that in the presence of magnetic field the transmission factors display also sensitivity to the projection of a spin to the field axis since the transition energy in channel i includes the energy difference

$$E_{\rm M} = (\mathcal{M}_J - \mathcal{M}_i - \mathcal{M}_I)B \tag{21}$$

of the field interaction with magnetic moments of compound nucleus $\mathcal{M}_J$ and reaction partners, i.e. for nuclei $\mathcal{M}_I$ and particles $\mathcal{M}_i$, in respective channel, $E_{iI}^\mu = E - S_i - E_I^\mu + E_{\rm M}$.

The individual particle transmission coefficients T_{m_l} are calculated by solving the Schrödinger equation with an optical potential for the particle-nucleus interaction. Many studies of thermonuclear reaction rates by Truran et al. (1966), Michaud & Fowler (1972), Arnould (1972), Truran (1972), Holmes et al. 1976 employed optical square well potentials combined with the black nucleus approximation. The local density approximation with the optical potential for neutrons and protons by Jeukenne, Lejeune, & Mahaux (1977), based on microscopic infinite nuclear matter calculations for a given density, have been incorporated by Thielemann et al. (1987). In addition, corrections of Fantoni et al. (1981), Mahaux (1982) to the imaginary part have been considered.

As extensively discussed by Thielemann et al. (1983), Cowan et al. (1991), Varner et al. (1991) the square well black nucleus approximation yields reasonable accuracy for s-wave neutron strength function $\langle \Gamma^o \mathcal{W} \rangle|_{1\mathrm{eV}} = (1/2\pi) T_{n(l=0)}(1\mathrm{eV})$. Such a limit implies negligible magnetic field effects in individual neutron transmission factors.

We note, in addition, that in such cases of predominant contribution from s-wave scattering the cross sections correspond to the condition $\sigma v \approx const$, and thermally averaged rates $r = \langle \sigma v \rangle$ vary only slightly in a wide range of temperatures, see Cowan et al. (1991). Therefore, in further evaluations of magnetic field effects we approximate the ratio of field dependent rate to the respective quantity at zero-field as a ratio of corresponding cross sections of radiative capture at neutron separation energies (see also Eq. (25) and discussion therein)

$$r(B)/r(0) \approx \sigma(B)/\sigma(0) \ . \tag{22}$$

The gamma-transmission coefficients are dominated by E1- and M1- gamma-transitions in total photon widths. The smaller, and consequently less important, M1 transitions have usually been treated with the simple single particle approach $T \propto E^3$ of Blatt & Weisskopf (1952), as also discussed by Holmes et al. 1976. The E1 transitions are usually calculated on the basis of the Lorentzian representation of the Giant Dipole Resonance (GDR). Within this model the E1 transmission coefficient for the transition emitting a photon of energy E_γ in a nucleus ${}^A_N Z$ is given by

$$T_{\mathrm{E1}}(E_\gamma) = \frac{8}{3}\frac{NZ}{A}\frac{e^2}{\hbar m_{\mathrm{N}} c^3}\frac{\Gamma_{\mathrm{GDR}} E_\gamma^4}{(E_\gamma^2 - E_{\mathrm{GDR}}^2)^2 + \Gamma_{\mathrm{GDR}}^2 E_\gamma^2} \ . \tag{23}$$

The spatial motion of nucleons determines GDR energies E_{GDR} and widths Γ_{GDR} which can be well described with semiclassical accuracy (see, e.g., Baran et al. 1996, Kondratyev & Di Toro 1996 and refs. therein). The Bohr-van Leeuwen theorem (van Leeuwen 1921, Terletskii 1939) suggests, indeed, that in classical limit the field effect can be omitted. This is also corroborated by more detail analysis (Kondratyev, Maruyama & Chiba 2000, Kondratyev 2001a) indicating only slight influence of magnetic fields of strengths considered here on nucleon spatial dynamics. Therefore, in specific calculations we adopt

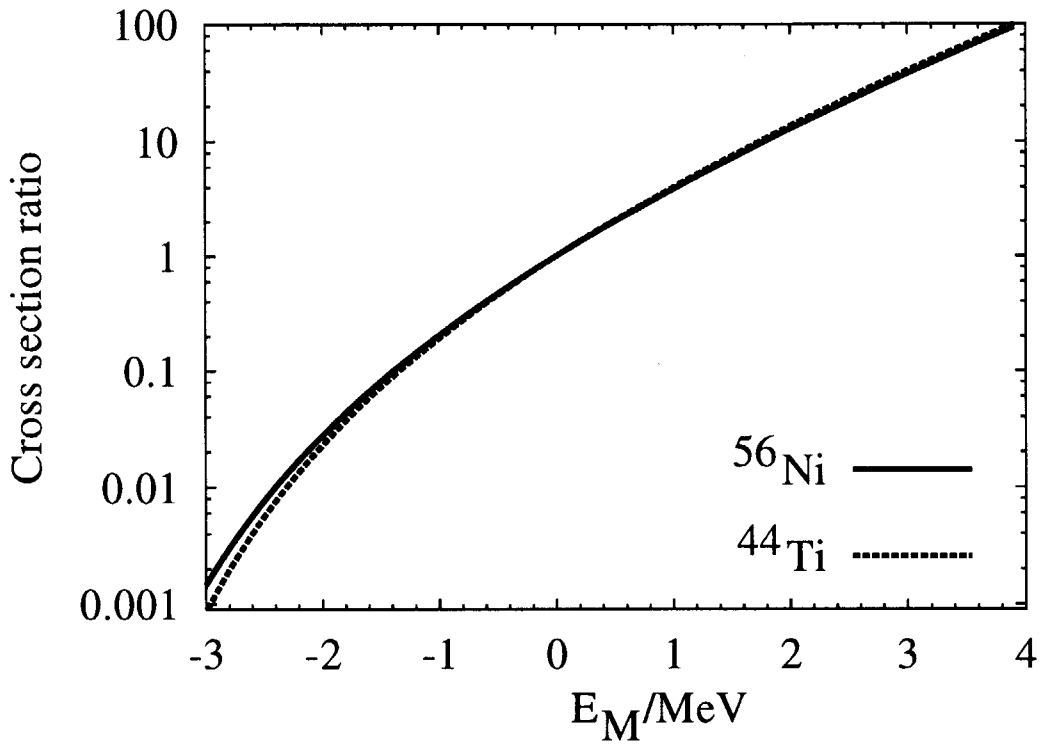

Fig. 6.— Effect of magnetic energy in radiative neutron capture cross section

E1 gamma-transitions with GDR energies and widths corresponding to laboratory conditions (Holmes et al. 1976)

$$E_{\rm GDR} \approx 35 \cdot A^{-1/6}\ {\rm MeV},\quad \Gamma_{\rm GDR} \approx 35 \cdot A^{-1/3}\ {\rm MeV}\ . \tag{24}$$

As seen in fig. 5 the E1-factor sharply rises at small energies and exhibits a maximum at about 19 MeV for nuclei of middle mass numbers. At thermal velocities such a behavior implies that the gain(lose) of γ-transition energy results in increase(decrease) of photon emission rate.

4. Radiative Neutron Capture in Magnetic Fields

As argued in sect. 3 important magnetic field effects in radiative capture processes are due to modifications of nuclear level densities and γ-transition energies. To illustrate the relationship between these mechanisms as well as the sensitivity to approximations we consider a schematic example of neutron capture by neutron-odd nucleus with spin 1/2 which yields exit channel even-even nucleus corresponding to vanishing values of the spin-projection at the Fermi energy $m_{\rm F} = 0$. Then for s-wave neutrons the field-projection of compound nucleus spin $m_J = 1$, since spins of neutrons and nuclei are i aligned along magnetic field. Selection rules for dipole γ-emission imply $m_J - m_O = m_\gamma$ with the photon-angular-momentum projection $m_\gamma = 0, \pm 1$. In this case Eq. (21) results

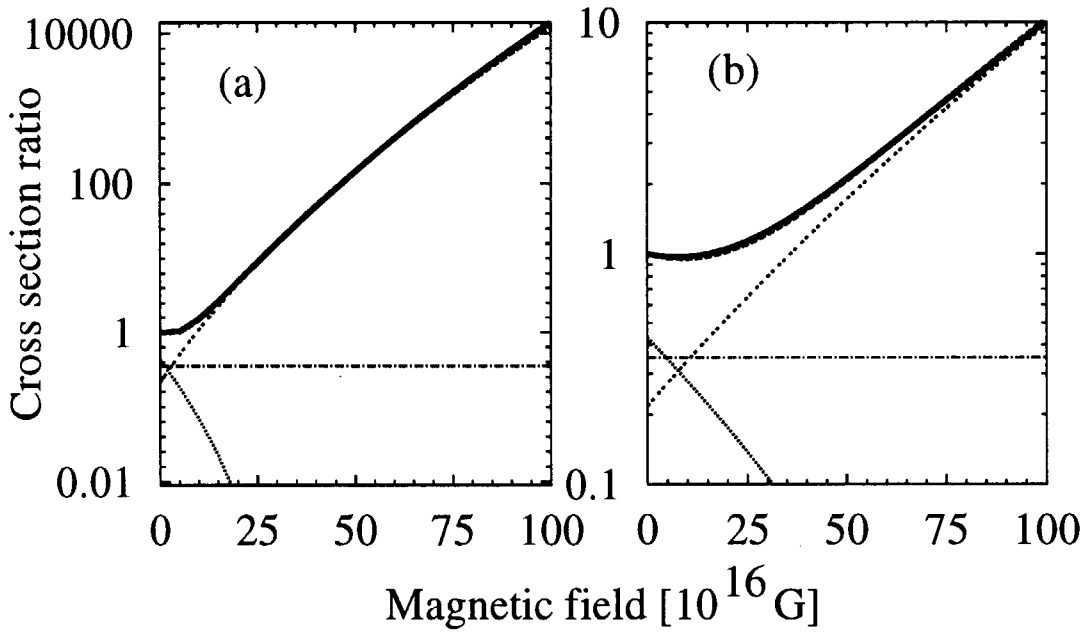

Fig. 7.— Effect of magnetic energy in radiative neutron capture cross section for $|g_{\rm eff}| = 3.8263$ (a) and 1 (b). The normalized at zero-field total cross section for ^{56}Ni and ^{44}Ti are indicated by thick solid and dashed lines, while thin dotted, dashed-dotted and double-dotted lines represent the partial contributions of ^{56}Ni states with spins 0, 1, and 2, respectively.

in magnetic energy $E_{\rm M} \approx g_{\rm eff}\mu_{\rm N}Bm_\gamma$, where an effective g-factor $g_{\rm eff}$ approaches the neutron value g_n for predominant contribution of active neutron in change of nuclear configuration, or unity for spatial mechanisms.

In further calculations we employ the ingredients of statistical model discussed above for cases of ^{44}Ti and ^{56}Ni. Furthermore, taking into account predominant contribution of neutron channel to total transmission coefficients in Eq. (7) at small velocities v_{nI} we approximate the cross section normalized at zero field by respective normalized γ-coefficient

$$\sigma(B)/\sigma(0) \approx T_\gamma(B)/T_\gamma(0). \qquad (25)$$

Incorporating the laboratory level density parameters we consider effect of magnetic energy $E_{\rm M}$ in n-capture process. As illustrated in fig. 6 positive or negative magnetic energy balance between entrance and exit channels leads to enhancement or suppression of the cross section, respectively. Nearly exponential energy dependence of the normalized at zero energy cross section points to predominant level density mechanism of this effect. Taking into account various spin-states in exit channel we see from fig. 7 that the contribution of magnetic energy $E_{\rm M}$ results in considerable enhancement of n-capture process in strong magnetic fields. The largest contribution of zero-spin states in out-channel

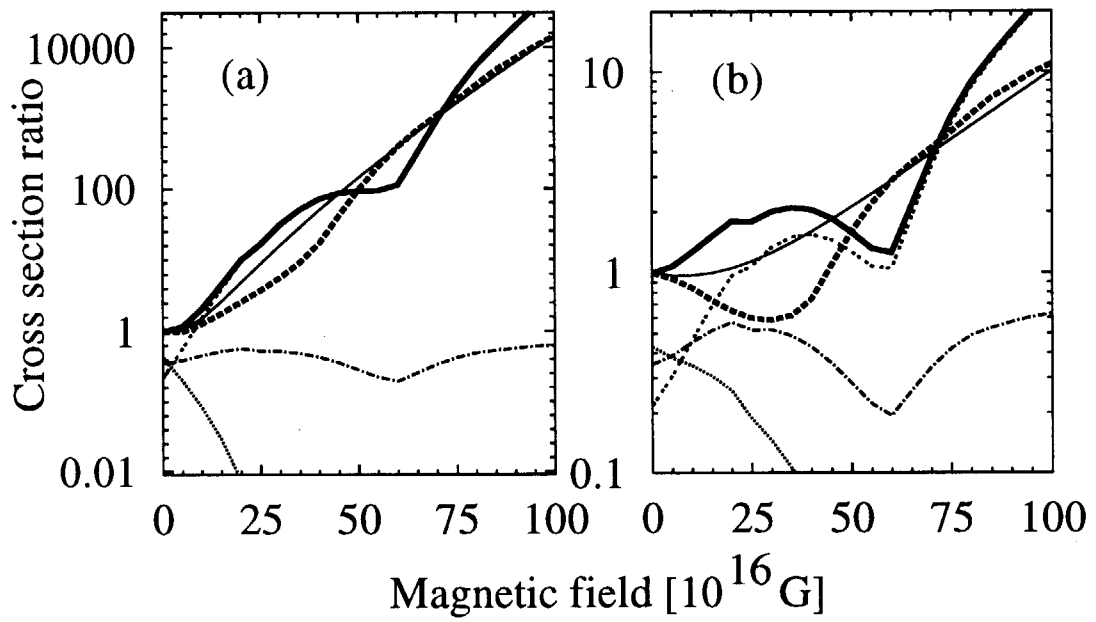

Fig. 8.— The same as in fig. 7 but including magnetic field effect in the level density. The thin solid line shows magnetic energy effect for ^{56}Ni from fig. 7.

at zero field sharply vanishes with increasing field strength, while the population of the highest allowed spin-states grows. This results in nearly constant cross section in weak field limit. In magnetic fields of large strengths such highest spin-states of final nuclei give predominant contribution to the total cross section because of large extra-energy in γ-channel. The cross section ratio is almost the same for both nuclei. The comparison of panels (a) and (b) in fig. 7 indicates that the enhancement is considerably stronger for larger values of g-factor.

The mechanisms due to magnetic effects in level densities and γ-energies are brought together in fig. 8. The magnetic change in level spacing is seen to result in oscillations of n-capture cross section around monotonic enhancement caused by magnetic energy. Contribution of such oscillations is particularly important for relatively small absolute values of g-factors. Preferable occupation of higher spin states for reaction product remains. We note that the field dependence of the level density brings varying cross section also for an unchanged spin projection. The magnetic effects in level spacing gives rise to considerably different cross section ratios for ^{56}Ni and ^{44}Ti nuclei. For the case of product-nucleus ^{56}Ni, with closed shell at zero-field, n-capture process displays an extra enhancement, while for ^{44}Ti the reaction can be suppressed at weak fields.

5. Magnetic Shift of Nuclear Magic Numbers

As we have seen in sect. 3 magnetic modification of shell closure properties of nuclear masses plays an important role in the field effects on nuclear reaction rates. In this section we analyze and systemize such properties by employing the shell model.

5.1. Magnetism of Nuclei within the Shell Model

As demonstrated by Kondratyev et al. (1999, 2000, 2001, 2002) thermodynamic formalism within the non-relativistic mean-field treatment constitutes useful framework for an analysis of the nuclide reactivity in magnetic fields of interest. Within the Hartree mean-field treatment (see, e.g., Kondratyev 2001, Bohr & Mottelson 1969, Nilsson & Ragnarsson 1990) the nuclear structure is described in terms of the single-particle (sp) levels ϵ_ζ filled up to the Fermi energy $\epsilon_{\rm F}$, which determine the properties of $N = \int_{-\infty}^{\epsilon_{\rm F}} {\rm d}\epsilon\ \rho(\epsilon)$ nucleons. Decomposing the sp level density $\rho(\epsilon) = \sum_\zeta \delta(\epsilon - \epsilon_\zeta) = \rho^{\rm sm} + \delta\rho$ into smooth $\rho^{\rm sm}$ and oscillating $\delta\rho$ components we express the energy of a nucleus as

$$E = \int_{-\infty}^{\epsilon_{\rm F}} {\rm d}\epsilon\ \epsilon\rho(\epsilon) = E^{\rm sm} + C_{\rm n} + C_{\rm p}\,, \tag{26}$$

where the Thomas-Fermi (i.e. semi-classical) component $E^{\rm sm}$ is only slightly affected by magnetic fields due to the Bohr-van Leeuwen theorem (van Leeuwen 1921, Terletskii 1939). The leading field effect is connected with shell-correction contributions (Kondratyev 2001, Strutinsky 1967, 1968) of neutrons $C_{\rm n}$ and protons $C_{\rm p}$ to nuclear masses which are related to the oscillating part $\delta\rho$.

Great success in the understanding of many properties of stable nuclei is associated with the Nilsson model (NM) (cf., e.g., Bohr & Mottelson 1969, Nilsson & Ragnarsson 1990) which is based on the Harmonic Oscillator (HO) confining potential approximation for the nuclear mean-field. In present study we consider the simplified NM spectra corresponding to spherical HO Hamiltonian

$$\epsilon_{nlj} = (n + 3/2) + \eta_{\rm so}\left\{\begin{matrix} -l \\ l+1 \end{matrix}\right\}\,, \quad \text{for } j = l \pm \frac{1}{2}\,, \tag{27}$$

where the spin-orbit (s-o) coupling constant $\eta_{\rm so} \approx 0.12$, and the energy is measured in units of the HO frequency ω_0. For nuclei in vicinity of stability line $\omega_0 \approx 41/A^{1/3}$ MeV, while neutron rich nuclei involved in the r-process network correspond to significantly smaller level spacing. Such an approximation provides accurate description for light and medium mass nuclei (Bohr & Mottelson 1969, Nilsson & Ragnarsson 1990).

Neglecting the s-o coupling yields the equidistant sp spectrum corresponding to principal quantum numbers n with level degeneracies $(n + 1)(n + 2)$. Such a picture of HO confinement might provide reliable description of neutron rich nuclides with considerably

suppressed s-o coupling (Haensel, Zdunik & Dobaczewski 1989, Oyamatsu & Yamada 1994, Ozawa et al. (2000)).

5.2. Pauli-spin Magnetization

The interaction of magnetic field with nucleon-spin-dipole magnetic moment leads to an additional term in the energy spectra

$$\delta\epsilon_{\rm i} = \sigma_i \Delta_\alpha \, , \; \Delta_\alpha = g_\alpha b/2 \tag{28}$$

with the g-factor g_α, and reduced field strength $b = \omega_{\rm L}/\omega_0$. Such a term contributes to sp energies of both protons $\alpha = {\rm p}$, and neutrons $\alpha = {\rm n}$, and gives rise to a relative shift down and up (see fig. 9b) of energy levels with the nucleon spin-magnetic moment directed along the field ($\sigma_{i=\uparrow} = -1$, majority-spin levels) and in the opposite direction ($\sigma_{i=\downarrow} = 1$, minority-spin levels), respectively. The shift, Eq. (28), is related to the Pauli-type of the magnetic response and modifies the shell-correction energy as

$$C_\alpha = C_\alpha^{\uparrow}(\epsilon_{\rm F} + \Delta_\alpha) + C_\alpha^{\downarrow}(\epsilon_{\rm F} - \Delta_\alpha) \, , \tag{29}$$

where C_α^i is determined by the unshifted sp spectrum (see Eqs. (26) and (27)).

The spin magnetization represents predominant effect in the magnetic field dependence of the neutron shell-correction energy and leads to a phase-shift of shell-oscillations (Kondratyev 2001). This behavior is caused by the field dependent interference of contributions coming from the majority- and minority-spin neutrons to the total energy. As illustrated in fig. 9a such an interference gives rise to oscillations of the shell-energy as a function of magnetic field strength with a period $b_{\rm s} \approx 0.5$, where the subscript s at defined above parameter b indicates that respective oscillation period corresponds to spin magnetization. Figure 9b indicates that for nearly stable nuclei the respective magnetic field $B_{\rm s} \sim \omega_0/\mu_{\rm N} \sim 10^{16} - 10^{17}$ G induces the relative shift $\Delta_{\rm n}$, Eq. (28), of neutron majority- and minority-spin energy levels which is comparable to the energy difference between major shells given by the HO frequency ω_0. In particular, at field strengths corresponding to the region near $b \approx |2g_{\rm n}|^{-1} \approx 0.26$ the level spacing and the degeneracies are decreased resulting in a suppression of the shell effect as compared to the values related to level crossings, $b_{\rm cr} = |k/g_{\rm n}|$ with an integer k.

At zero-field the pronounced minima are displayed at neutron numbers, $N_{\rm m}^0 = 8$, 20, 40, 70, 112, 168, ..., associated with closed shells, as extensively discussed in, e.g., ref. (Bohr & Mottelson 1969). In the case of $b \approx |1/g_{\rm n}|$ the level spacing and the shell-oscillation amplitude are nearly the same as at $b \approx 0$. However, as indicated in fig. 9b level occupation numbers are rather different in these two cases. Consequently, the positions of shell-energy minima are replaced. At the field strength matching the first level crossing the familiar spherical HO magic numbers are turned into anti-magic, i.e.

associated with positive maxima of the shell-correction energy, while the open shell anti-magic numbers become the closed shell magic numbers. For grand canonical ensemble the field dependence of the shell energy minima can be obtained from the condition of constant arguments in Eq. (29). This yields an approximation

$$N_{\rm m}^{\pm}/N_{\rm m}^{0} \approx (1 \mp g_{\rm n} b/2(3N_{\rm m}^{0})^{1/3})^{3}\,, \tag{30}$$

where $\pm$ corresponds to upper and lower valleys extending from the respective zero-field magic numbers $N_{\rm m}^{0}$ (see fig. 9a). As evident from fig. 9a linear term dominates such a dependence. We note that magic number of canonical ensemble deviate from the case of grand canonical by about 1% and 5% at the first and second level crossings, respectively.

The effect of a sign change in the shell-correction energy remains when accounting for the spin-orbit interaction as well (Kondratyev 2001). Furthermore, the sign inversion occurs at the field strength that is almost an order of magnitude smaller than the oscillation period $B_{\rm s}$ (see above).

5.3. Orbital Magnetism

The interaction of magnetic field with proton charge moving along the confined trajectory gives rise to an additional modification of proton spectra which at small field strengths $b \ll 1$ reads

$$\delta\epsilon_{\rm o} \approx b l_3\,, \tag{31}$$

where l_3 denotes the projection of the proton angular momentum on the field axis. Switching off the Pauli response, i.e. $\Delta_{\rm p} = 0$ in Eq. (29), the properties of the orbital magnetism can be easily seen by employing the simplified expression for the shell-correction energy at conditions of weak fields in the form (see Kondratyev 2001, Kondratyev & Lutz 1998)

$$C_{\rm o}^{i} \approx -\frac{\omega_0 X(X+1)}{8\pi^4} \sum_{k=1} k^{-2} \cos(kX) j_0(bkX)\,, \tag{32}$$

where $X = 2\pi\epsilon_{\rm F}/\omega_0 \approx 2\pi(3N)^{1/3}$ counts the number of filled shells in zero-field limit. The effect of orbital magnetism consists, therefore, in a modulation of components for a nonperturbed spherical HO by the spherical Bessel function with the field dependent argument. As indicated by Eq. (32) and illustrated in fig. 10 the weak field leads to regular oscillations of the shell-correction energy as a function of the field strength as well as overall suppression the shell effect with increasing b at zero s-o coupling. As seen in fig. 10 local maxima of the shell-energy amplitude arise along the lines

$$Z^{p} \approx [(p+1/2)/2b]^{3}/3 \tag{33}$$

with an integer p. The shell-correction component vanishes when in Eq. (33) $p = k + 1/2$ at integer k. Therefore, orbital magnetism yields the oscillation period $b_{\rm o} \approx X^{-1} \sim A^{-1/3}$

corresponding to the field strength $B_o = \omega_0/\mu_N X \sim A^{-2/3}$. This estimate (cf. also fig. 10) yields a weaker field for heavier nuclei in order to invert the sign of the proton shell-correction energy as well as to wash out the shell-structure. The minima valleys in shell-correction energy landscape follow the lines

$$Z_m^{\pm}/Z_m^0 \approx [(1 \mp b_m)/(1 \mp b)]^3\,,\; b_m = 1/(4(3Z_m^0)^{1/3})\,, \tag{34}$$

with a good accuracy up to the third oscillation.

5.4. Paramagnetism versus Orbital Magnetism of Protons in Nuclei

The magnetic field dependence of the proton shell-correction energy is given as a combination of the discussed in sect. 5.2, fig. 9 and Eq. (29), Pauli-magnetism and the Landau-type of orbital magnetism related to proton ballistic dynamics (see fig. 10 and Eqs. (31) and (32)). Switching on the spin-magnetic response we obtain the proton shell-correction energy which is shown in fig. 11 as a function of the proton number Z and magnetic field strength b. As seen the damped oscillations of the shell energy correspond to the period b_{so} decreasing with the mass number similarly to a pure orbital magnetism. The Pauli-type magnetization reduces, however, additionally the field strength that is required to change the sign in the proton shell-correction energy. The phase-shift on π (i.e. the reversed sign) occurs at the parameter b which is considerably smaller than the value $1/g_p$. The interplay between the Landau-type and spin-magnetism gives rise to an extra-decrease of the period of a sign oscillation. The relevant field strength is, therefore, smaller than the corresponding field for neutrons by a factor exceeding the ratio $|g_p/g_n|$. At the Fermi energy the respective magnetic field shifts the proton majority- and minority-spin levels on an energy $(\delta\epsilon_i + \delta\epsilon_o)$ comparable to the HO level spacing ω_0. The energy of the first Landau level ω_L is, however, by the factor 6 – 7 smaller than the energy difference between the major shells, while the radius of the proton cyclotron orbit is larger than the radii of nuclei on approximately the same factor. Consequently, Landau levels give almost no contribution to the magnetism of nuclei. The orbital magnetism in such a case is mainly given by an interaction of the magnetic field with the magnetic dipole arising from the quantum orbital motion of protons inside the nucleus. The orbital magnetic response of such an inhomogeneous system is considerably amplified as compared to the magnetism of a homogeneous liquid which originates from the quantization of proton orbital motion in magnetic field. The Landau levels are expected to contribute noticeably to the magnetic response when their and nuclear radii become comparable. Corresponding field strength $B_L \sim 10^{19}$ G.

As seen from the comparison of Figures 9, 10 and 11 the interplay between spin and orbital magnetic reactivities yields more complicated proton shell-correction energy landscape as compared to their independent responses in a field. In this case the magnetic

field evolution of the proton shell-energy valleys can be guided by the lines

$$Z^{\pm}_{\rm m}/Z^{0}_{\rm m} \approx ([(1 \mp b_{\rm m})/(1 \mp b)] \pm g_{\rm p} b/2(3Z^{0}_{\rm m})^{1/3})^{3} \qquad (35)$$

which represent a combination of Eq. (30), but with proton g-factor $g_{\rm p}$, and Eq. (34). As illustrated in fig. 11 the valleys display irregular shapes passing from upper to lower lines.

It is worthy to recall here that the presence of s-o interaction leads, in addition, to an anomalous field dependence of the proton shell-correction energy amplitude (Kondratyev 2001). The proton orbital magnetism yields rather pronounced enhancement of the shell effect. Especially, when the values of the parameter b are close to the spin-orbit strength $\eta_{\rm so}$, the shell-oscillation amplitude can be considerably amplified.

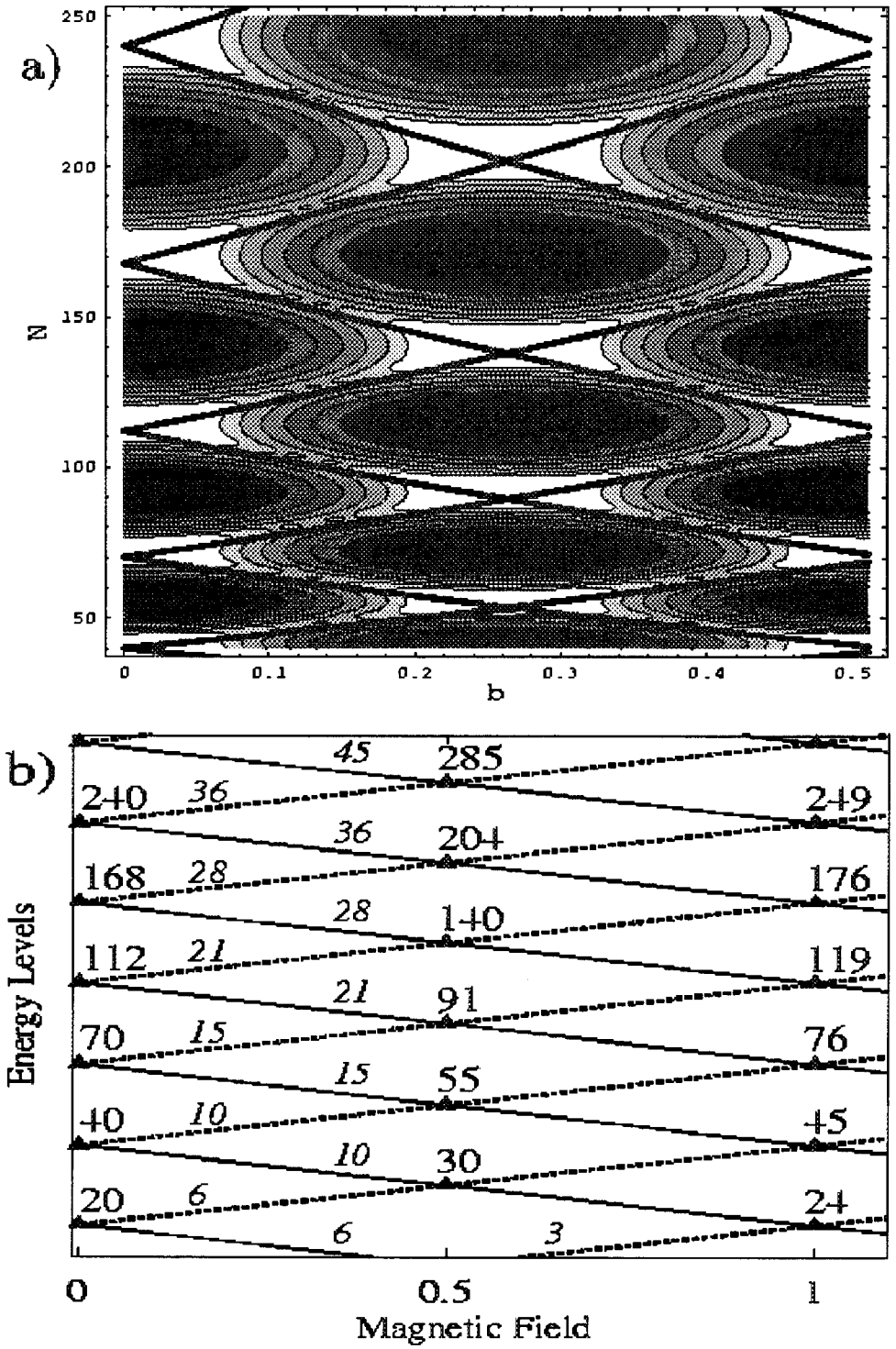

Fig. 9.— a) Spherical HO model prediction of the neutron shell-correction energy versus the neutron number N and the parameter b. Smaller energies are indicated by white regions, while the dark regions denote larger energies. The contours are plotted with the step 0.5 starting from -1.5 for the quantity $C_n \cdot 8\pi^4/(\omega_0 X^2)$. The thick solid lines are related to the relationship Eq. (30). b) The dependence of the majority- (solid lines) and minority-spin (dashed lines) energy level on the magnetic field. The energy and the field are measured in the units of the HO level spacing ω_0 and $[\omega_0/g_n\mu_N]$, respectively. The figures at the level crossings (indicated by triangles) show the total nucleon number when the levels are filled starting from the bottom. The level degeneracies are displayed by the numbers attached to respective lines.

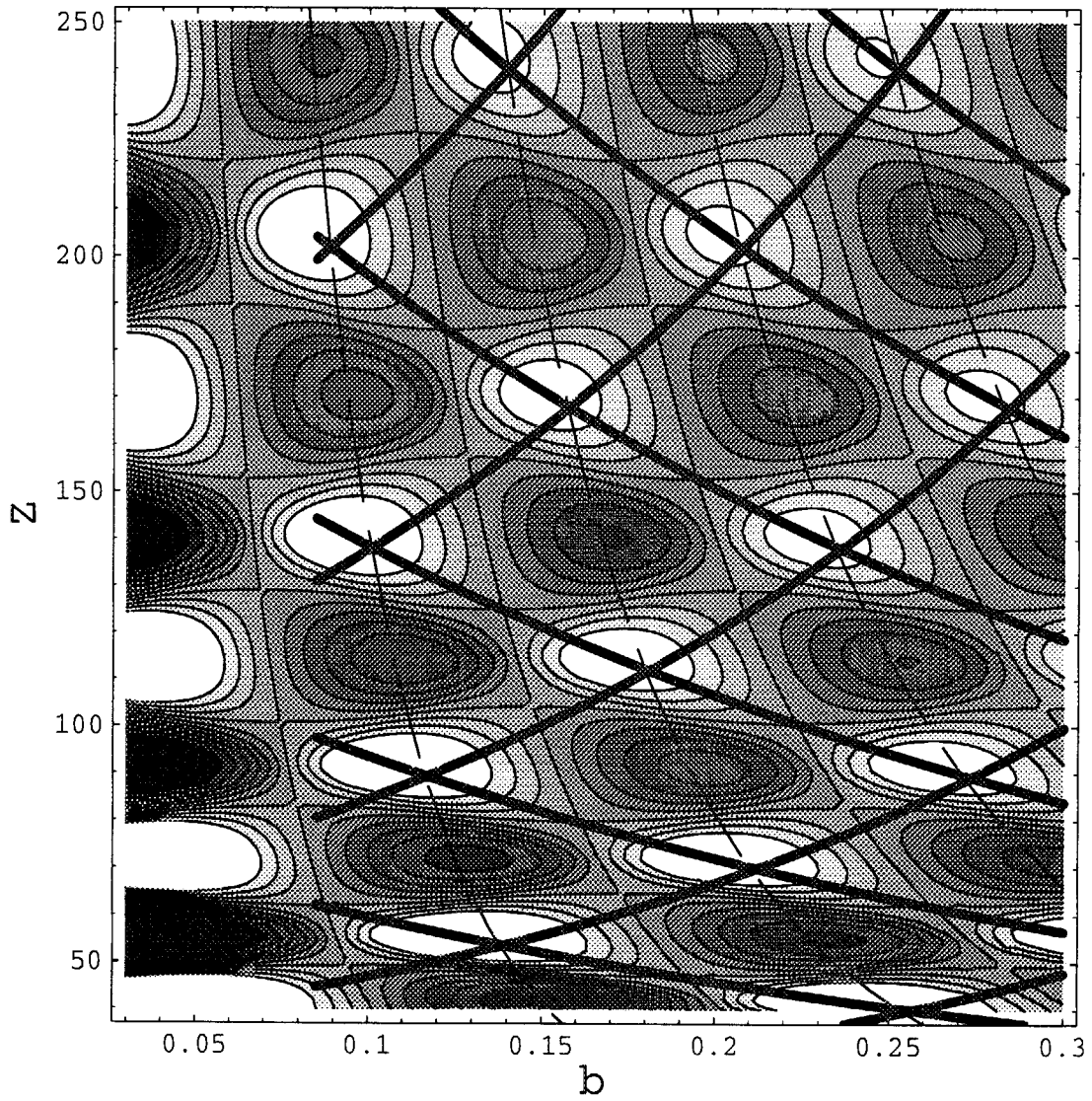

Fig. 10.— Effect of orbital magnetism in the proton shell-correction energy versus the proton number Z and the parameter b for the spherical HO potential. The white regions display to the energy minima (i.e. the wells), while the dark regions indicate the maxima (i.e. the hills) in the shell-correction energy landscape. The contours are plotted with the step 0.15 starting from -1 for the quantity $C_{\rm p} \cdot (1 + b/b_0)8\pi^4/(\omega_0 X^2)$, where $b_0 = (4 \cdot 90^{1/3})^{-1} \approx 0.056$. Thick solid lines represent Eq. (34), while dashed lines correspond to Eq. (33).

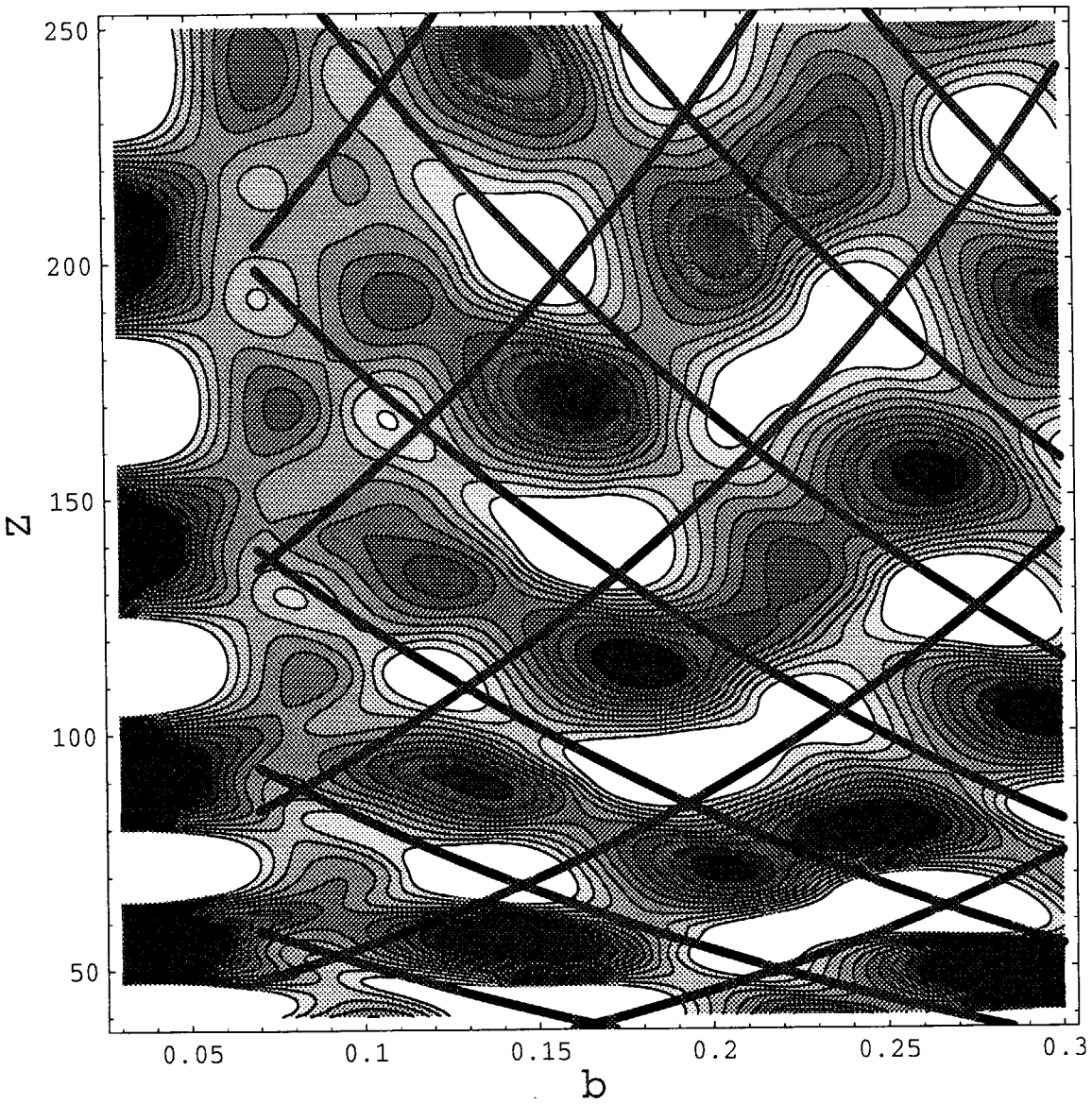

Fig. 11.— Spherical HO model prediction for the magnetic field dependent proton shell-correction energy when including spin and orbital magnetization. The contours are the same as in fig. 10, while thick solid lines are associated with Eq. (35).

6. Implications in the R-process

The rapid neutron-capture process (i.e. r-process) proceeds through the syntheses of highly unstable nuclei approaching the neutron drip-line and operates via nuclear transformations governed by strong, electromagnetic and weak interactions. Such nuclear reaction network involves mainly neutron captures, (γ, n)-photodisintegrations, β-decays and beta-delayed processes. The large neutrino-flux from nascent neutron stars may possibly play a role in nuclear reaction network, as well. The interplay between nuclear structure far from beta-stability line and certain astrophysical environment originates the r-process abundances. In fact, generation of heavy r-process nuclei requires an excess of 10 neutrons per seed nucleus in iron mass region or slightly beyond.

Observations of heavy elements in low metallicity stars with Fe/H abundances ranging between 0.1 % and 1 % from the solar one provide an information on stellar surface compositions displaying, thereby, interstellar gas components which form the stars at early stage of galactic evolution. Such observations show, on one hand, abundance patterns rather similar to solar r-process (at least for mass numbers $A > 130$) indicating, thereby, that during such early times in galactic evolution mainly r-process sources contribute to the production of heavy elements (Sneden et al. 1996, Cowan et al. 1997) while almost no s-process sources are involved. Consequently, in low and intermediate mass stars the s-process sets in only during late evolution time exceeding 10^8 y.

At the same time, it is recognized that for reaction rates evaluated on the basis of laboratory data the r-process nuclear assembly arise with a delay of over 10^7 y after iron and oxygen nuclei (Mathews, Bazan, & Cowan 1992). Such a condition potentially controvert to an inclusion of the large mass SNe II to candidates of r-process site, because of short evolution time of such stars with masses beyond 10-12 $M_\odot$. The r-process is generally associated with the inner ejecta of type II supernovae (see, e.g., reviews by Cowan et al. (1991) and Meyer (1994)), but also the decompression of neutron star matter was suggested by Lattimer et al. (1977), Meyer (1989), and Eichler et al. (1989) and is consistent with the above mentioned low metallicity observations. Both these environments provide or can possibly provide high neutron densities and high temperatures.

Models trying to explain the whole r-process composition by low neutron density ($\mathcal{D}_n < 10^{20}\,\mathrm{cm}^{-3}$) and temperature ($T < 10^9\,\mathrm{K}$) environments, like explosive He-burning in massive stars by Thielemann et al. (1979), are at least questionable according to Blake et al. (1981). The high entropy wind from the hot neutron star following type II supernova explosions has been suggested as a promising site for r-process nucleosynthesis by Woosley & Hoffman (1992), Woosley et al. (1994b), and Takahashi et al. (1994). Magnetic enhancement of nuclear reaction rates may serve as a source of entropy enhancement.

Actual r-process calculations employ usually two different approaches. Focusing mainly

on nuclear physics issues far from stability one group of studies make use of a model-independent approach for the r-process as a function of neutron number densities $\mathcal{D}_n$ and temperatures T, extending for a duration time τ (see e.g. Kratz et al. (1988), Kratz et al. (1993), Thielemann et al. (1994a), Chen et al. (1995), Bouquelle et al. (1996), Pfeiffer et al. (1997), and Kratz et al. (1997)). Another studies usually concentrate on specific astrophysical environment and follow the expansion of matter on typical time-scales τ with an initial entropy, passing through declining temperatures and densities until the freeze-out of all reactions (see, e.g., Woosley and Hoffman (1992), Meyer et al. (1992), Howard et al. (1993), Hoffman et al. (1996), Qian & Woosley (1996), Hoffman et al. (1997), Meyer & Brown (1997ab), and Surman et al. (1997)). In this section we briefly discuss magnetic field effects in r-process.

6.1. The Canonical R-process Path

The actual r-process path is governed by the sequence of neutron captures, (γ, n)-photodisintegrations and beta-decays (and likely additional reactions like beta-delayed neutron emission, fission etc.) which are in principle determined by detailed reaction network described by a system of (several thousand) coupled differential equations with a dimension equal to the number of isotopes. This can be resolved efficiently as shown by Cowan et al. (1991). However, at neutron densities and temperatures exceeding considerably the values $\mathcal{D}_n > 10^{20}\,\mathrm{cm}^{-3}$ and $T > 10^9\,\mathrm{K}$, the short capture reaction time-scales ($\approx 10^{-4}\,\mathrm{s}$), see, e.g., Cameron et al. (1983), Bouquelle et al. (1996), and Goriely & Arnould (1996), justify further simplifications, since the beta-decay half-lives are considerably longer (roughly of the order of $10^{-1}\,\mathrm{s}$ to a few times $10^{-3}\,\mathrm{s}$). Such a case brings equilibrated neutron capture and photodisintegration processes. These conditions allow to make use of the 'waiting point approximation', sometimes also referred for as the 'canonical r-process', which is equivalent to an $(n,\gamma) \rightleftarrows (\gamma, n)$–equilibrium. This approximation relates n-capture and photon induced neutron emission rates as well as the abundances $Y_{(Z,A)}$ as

$$r_{n,\gamma}^{Z,A} Y_{(Z,A)} = \lambda_{\gamma,n}^{Z,A+1} Y_{(Z,A+1)} \tag{36}$$

for all nuclei in an isotopic chain with charge number Z. The photodisintegration rate $\lambda_{\gamma,n}^{Z,A+1}$ is related to the n-capture rate $\langle \sigma v \rangle_{n,\gamma}^{Z,A}$ by detailed balance (Fowler et al. 1967)

$$\lambda_{O,\gamma}(T) = \left(\frac{G_n G_I}{G_O}\right)\left(\frac{A_I}{A_O}\right)^{3/2}\left(\frac{m_\mathrm{N} k_\mathrm{B} T}{2\pi\hbar^2}\right)^{3/2} \langle \sigma v \rangle_{In} \exp\{-Q_{In}/k_\mathrm{B}T\}. \tag{37}$$

This expression depends on the reaction Q-value associated with respective particle separation quantities Q_{In}, the temperature T, and the mass numbers A of the participating nuclear particles in a thermal bath of temperature T. We note that at vanishing magnetic fields the neutron partition function $G_n = 2$, see Eq. (4).

As seen from Eqs. (36) and (37) the maximum abundance in each isotopic chain (where $Y_{(Z,A)} \approx Y_{(Z,A+1)}$) is located at the same neutron separation energy S_n, being the neutron-capture Q-value of nucleus (Z, A). When less important effects, like ratios of partition functions, are neglected the location of the r-process path, i.e. the contour lines of neutron separation energies corresponding to the maximum in all isotopic chains, can be expressed in terms of the neutron number density $\mathcal{D}_n$ and the temperature T in an astrophysical environment, as reviewed by Cowan et al. (1991).

Such r-process paths are responsible, e.g., for the solar r-process abundances. The respective nuclear network proceeds via highly neutron-rich, unstable nuclei which are located $15 - 35$ units away from β-stability line and correspond to neutron separation energies of order of $S_n = 2 - 4$ MeV. These are predominantly nuclei which are not easily accessible in laboratory experiments to date. The particularly important regions of the closed shells N=50 and 82, where continuous efforts are taken to extend experimental information in vicinity of mass numbers $A = 80$ and 130 with radioactive ion beam facilities (cf., e.g., Ozawa et al. (2000) and discussion therein).

The dependence on nuclear masses or mass model predictions enters via neutron separation energy S_n. The beta-decay properties along contour lines of constant S_n towards heavy nuclei (see, e.g., Fig. 4 in Thielemann et al. (1994a)) are responsible for the resulting abundance pattern. At conditions of canonical r-process (i.e. waiting point approximation) the formation of heavy nuclei is governed by effective decay rates λ_β^Z of isotopic chains. Then the environment properties $\mathcal{D}_n$ and T (defining the S_n for the path) and the duration time τ determine the resulting composition of nuclear spices. In case of sufficient duration time τ (i.e. longer than the longest half-lives encountered in such a path) the following steady flow of beta-decays results in abundance ratios independent on duration τ. The saturated composition corresponds to $\lambda_\beta^Z Y_{(Z)} \approx const$ for all Z-isotopic chains, where $Y_{(Z)}$ is the total abundance of an isotopic chain and λ_β^Z represents its effective beta-decay rate.

Number of idealizations in this picture has to be pointed out. The assumption of independence of separation energies S_n on astrophysical parameters over the duration time τ implies that nuclei exist in forms of highly unstable isotopes which decay back to beta-stability. In reality $\mathcal{D}_n$, and T exhibit the time and spatial dependence. As long as $\{\mathcal{D}_n, T\}$ are high enough to ensure the waiting point approximation, one can neglect the memory effects during evolution, because of lack memory in the system which immediately adjusts to proceeding equilibrium conditions and only the new values $(\mathcal{D}_n, T)$ are important. The prominent question is whether the decrease from equilibrium conditions in $\mathcal{D}_n$ and T which initially ensure the waiting point approximation, down to conditions where the competition of neutron captures and beta-decays has to be taken into account explicitly (neutron freeze-out) can affect significantly resulting abundances. Investigations usually

consider sudden drop in $\mathcal{D}_n$ and T, leading to a sudden 'freeze-out' of the abundance pattern, while only beta-decays and beta-delayed processes (like, neutron emission and fission) are accounted for the final decay towards the vicinity of stability line (see e.g. the effect displayed in Fig. 9 of Kratz et al. (1993)).

When applying such a strategy, an analysis of the solar-system isotopic r-process abundance pattern shows that as a minimum three components with different neutron separation energies S_n (characterizing in turn different r-process paths) are required in order to reproduce correctly three peaks at $A \simeq 80$, 130, and 195 and the abundances between them (Thielemann et al. (1993), Kratz et al. (1993)). When making use of experimental beta-decay properties at magic neutron numbers $N = 50$ and 82, as well as the abundance pattern down to the next peak, the low mass number A components of the peaks could be properly reproduced even with the assumption of a steady flow of beta-decays. Such an agreement indicates that the astrophysical duration time-scales τ are large as compared to the most of beta-decay half-lives encountered in the synthesis. At the same time it suggests that the time is only comparable to the longest half-lives in the peaks, where the path exhibits the closest approach to the stability line, and which control, in fact, the leaking out to larger mass numbers A. The continuous superposition (rather than only three, as expected in astrophysical environment) of components with varying $\mathcal{D}_n$, T or $S_n(\mathcal{D}_n, T)$ with equidistant steps in separation energy S_n between 2 and 4 MeV and τ between 1 and 2.5 s led to a slight (but not dramatic) change/improvement of the abundance curve in Kratz et al. (1994).

When the calculations of Kratz et al. (1993) were supplemented by use of the most modern mass formula data, i.e. Finite Range Droplet Model (FRDM) by Möller et al. (1995) and Extended Thomas-Fermi model with Strutinsky Integral (ETFSI) by Aboussir et al. (1995), instead of using a somewhat dated but still very successful droplet model by Hilf, von Groote, & Takahashi (1976), one could show that abundance troughs appeared before (and after) the 130 and 195 abundances peaks, due to specific behavior of the contour lines for quantities S_n of these mass models (Thielemann et al. (1994a), Chen et al. (1995)). The location in N of an r-process path with a given S_n does not behave smoothly as a function of Z. Sudden jumps are displaied at positions of magic neutron numbers, where the contour lines show a saddle point behavior for the FRDM as well as ETFSI mass models. The population gap of nuclei as a function of A leads after decay to the abundance.

Additional tests were performed in order to see how this pattern could be avoided with different nuclear structure properties far from stability. One possibility to overcome the problem has been considered by Chen et al. (1995). For very neutron-rich nuclei the shell gap at the magic neutron number $N = 82$ is less pronounced, i.e. quenched, than predicted by the global macroscopic-microscopic mass models. For light nuclei the

quenching of shell effects in neutron-rich isotopes represents an established and long-studied property (see, e.g., Orr (1991), Campi et al. (1975), Fukunishi, Otsuka, & Sebe (1992), and Sorlin et al. (1993)). The Hartree-Fock-Bogoliubov calculations by Werner et al. (1994), Dobaczewski et al. (1994), and Dobaczewski, Nazarewicz, & Werner (1995) with a specific Skyrme force yield suppression effects which were expected for the r-process path and i the result in proper abundance curve, as shown in Chen et al. (1995). This effect has been recently also confirmed by Pearson et al. (1996), when the ETFSI mass formula was phenomenologically quenched in a similar way as the HFB results and led to a very good agreement with solar r-abundances in a more systematic study by Pfeiffer et al. (1997). An experimental investigation of shell quenching along the $N = 50$ and 82 shell towards more neutron-rich nuclei (and approaching the r-process path for $N = 126$) is a highly desirable goal in order to test the nuclear structure responsible for the solar abundances of heavy nuclei.

6.2. Magnetic Shift of R-process Path

There are strong indications pointing to type II supernovae as r-process astrophysical site. However, galactic evolution time-scales suggest that r-process can perhaps efficiently operate only in the low mass SNe II with longer evolution time interval Cowan et al. (1991), Mathews et al. (1992), while neutron star mergers or still other sites are not necessarily excluded Lattimer et al. (1977), Meyer (1989), Eichler et al. (1989). As mentioned in sect. 1 the core region of massive SNe II can experience very strong magnetic fields. In this section we briefly analyze the field effect on r-process path.

Implications of simplified treatment to actual astrophysical sites rise the question on type of environment which satisfies the required conditions as well as on validity of sudden freeze-out approximation for realistic evolution time-scales encountered in specific environment. As shown in sect. 4 including the magnetic field enhances significantly the relevant reaction rates at the same values of density-temperature parameters $\{\mathcal{D}_n, T\}$. Such a property implies wider range of conditions for applicability of simplified canonical r-process picture as compared to the case of vanishing field limit.

In the ultramagnetized stellar media the detailed balance equations (Fowler et al. 1967) are modified to be

$$\lambda_{O,\gamma}(T) = \left(\frac{G_n G_I}{G_O}\right)\left(\frac{A_I}{A_O}\right)^{3/2}\left(\frac{m_{\rm N} k_{\rm B} T}{2\pi\hbar^2}\right)^{3/2}\langle\sigma v\rangle_{In}\exp\{-(Q_{In}+E_{\rm M})/k_{\rm B}T\}. \qquad (38)$$

The reaction Q-value includes, in addition to the field dependent particle separation quantities Q_{In}, the magnetic energy $E_{\rm M}$, see Eq. (21) and discussion therein.

As evident from Eq. (38) the r-process path in magnetized stellar media is determined by relationship between neutron separation $S_n(B)$ and magnetic $E_{\rm M}$ energies.

As discussed in sect. 5 predominant magnetic field effects in nuclear binding energies are associated with the oscillating (i.e. shell correction) parts. For neutrons the magnetic field dependence of shell energy exhibits an oscillating behavior displaying, thereby, magic-antimagic switching in nuclear structure. Consequently, the magnetic shift of magic numbers gives rise to the shift of saddle points in respective contour lines of r-process path. Furthermore, as demonstrated in sect. 4 magnetic fields enhance considerably population of high spin states of radiative capture reaction products. Therefore, the magnetic path might be shifted towards high spin states encreasing, thereby, the portion of large mass numbers.

7. Summary and Outlook

We have considered for the first time radiative nuclear capture reactions in ultra-magnetized stellar media relevant for supernova cores and neutron stars. Employing statistical model the magnetic field influence on the nuclear level densities and γ-transition energies is argued to dominate the field effect in the reactions. The nuclear structure is reflected by level densities which result in oscillations of radiative n-capture rate as a function of magnetic field strength. The interaction of the field with magnetic moments of nuclei modifies the photon energy, and enhances (n,γ) reaction cross sections as well as components of high spin states of reaction products. Such an enhancement suggests weaker conditions (i.e. neutron density and temperature) for applicability of nuclear synthesis 'waiting point' (or 'canonical r-process') approximation (Fowler, Caughlan & Zimmerman 1967,Fowler 1984, Meyer & Brown 1997, Hoffman et al. 1999) corresponding to $(n,\gamma) \rightleftarrows (\gamma,n)$ equilibrium. Furthermore, an increase in the population of high-spin states implies growing portion of massive nuclear spices. The detail evaluations require, however, to account for magnetic field dependence of spins of nuclei (cf., e.g., Kondratyev 2001, 2001a).

We note finally that similar magnetic effects can arise in electronic shell structure of magnetized atomic clusters (see, e.g., Kondratyev & Lutz 1998, 1999 and refs. therein). These phenomena have to be accounted in respective chemical processes.

Acknowledgments. This work was carried out under a strong leadership of Dr. Satoshi Chiba, the Group-leader of the Research Group for Hadron Science, who was so kind to give the author a chance to stay in JAERI for 3 years and provided him many important scientific guidances. The author is also greateful to Dr. Satoshi Chiba for excellent supports in daily life and providing the superb working condition which was inevitable in completing this work. He also wishes to thank the members of Research Group for Hadron Science and Advanced Science Research Center of JAERI for the warm hospitality, and to Dr. R.D. Hoffman for encouraging comments.

REFERENCES

Aboussir, Y., Pearson, J. M., Dutta, A. K., & Tondeur, F. 1995, At. Data Nucl. Data Tables, **61**, 127

Arnould, M. 1972, A & A **19**, 92

Baran, V., Colonna, M., Di Toro, M., Guarnera, A., Kondratyev, V.N. & Smerzi, A. 1996, Nucl. Phys. A **599**, 29c

Bethe, H.A. 1936, Phys. Rev. **50** 332

Blake, J.B., Woosley, S.E., Weaver, T.A., Schramm, D.N. 1981, Ap. J. **248**, 315

Blatt, J.M., & Weisskopf V.F. 1952, Theoretical Nuclear Physics (Wiley, New York)

Bloch, C. 1954, Phys. Rev. **93** 1094

Bohr, A. & Mottelson, B.R. 1969, Nuclear Structure (Benjamin, NY)

Bouquelle, V., Cerf, N., Arnould, M., Tachibana, M., & Goriely, S. 1996, A & A **305**, 1005

Broderick, A., Prakash, M., & Lattimer, J.M. 2000, ApJ, 537, 351

Cameron, A.G.W., Cowan, & J., Truran, J.W. 1983, Astopys. Space Sci. **91**, 235

Campi, X., Flocard, H., Kerman, A.K., Koonin, S. 1975, Nucl. Phys. A **251**, 193

Chen, B., Dobaczewski, J., Kratz, K.-L., Langanke, K., Pfeiffer, B.,Thielemann, F.-K., Vogel, P. 1995, Phys. Lett., Bi **355**, 37

Cowan, J. J., Thielemann, F.-K., Truran, J. W. 1991, Phys. Rep. **208**, 267

Cowan, J.J., McWilliam, A., Sneden, C., & Burris, D.L. 1997, Ap. J., **480**, 246

Dobaczewski, J., Hamamoto, I., Nazarewicz, W., Sheikh, J. A. 1994, Phys. Rev. Lett. **72**, 981

Dobaczewski, J., Nazarewicz, W., Werner, T. R. 1995, Phys. Scr. T **56**, 15

Duncan, R.C., & Thompson, C. 1992, ApJ, **392**, L9

Eichler, D., Livio, M., Piran, T., Schramm, D. N. 1989, Nature, **340**, 126

Fantoni, S., Friman, B.L., & Pandharipande, V.R. 1981, Phys. Rev. Lett. **48**, 1089

Feroci, M., Hurley, K., Duncan, R.C., & Thompson, C. 2001, ApJ, **549**, 1021

Feshbach, H. 1992, Theoretical Nuclear Physics. Nuclear Reactions (John Wiley & Sons, New York)

Fowler, W.A. 1984, Rev. Mod. Phys. **56**, 149

Fowler, W. A., Caughlan, G. E., & Zimmermann, B. A. 1967, Ann. Rev. Astron. Astrophys. bf 5, 525

———. 1975, Ann. Rev. Astron. Astrophys. **13**, 69

Fukunishi, N., Otsuka, T., & Sebe, T. 1992, Phys. Lett. B **296**, 279

Gilbert, A., & Cameron, A.G.W. 1965, Can. J. Phys. **43**, 1446

Goriely, S., & Arnould, M. 1996, A & A **312**, 327

Gotthelf, E.V., Vasisht, G., & Dotani, T. 1999, ApJ, **522**, L49

Haensel, P., Zdunik, J.L. , & Dobaczewski, J. 1989, A&A, 222, 353

Hauser, W., & Feshbach, H. 1952, Phys. Rev. A **87** 366

Hilf, E. R., von Groote, H., & Takahashi, K. 1976, in Proc. 3rd Int. Conf. on Nuclei far from Stability, Geneva, CERN-Rep 76-13, p.142

Hoffman, R. D., Woosley, S. E., Fuller, G. M., Meyer, B. S. 1996, Ap. J. **460**, 478

Hoffman, R. D., Woosley, S. E., Qian, Y.-Z. 1997, ApJ **482**, 951

Hoffman, R.D., Woosley, S.E., Weaver, T.A., Rauscher, T. & Thielemann, F.-K. 1999, ApJ **521**, 735

Holmes, J., Woosley, S., Fowler, W., & Zimmerman, B. 1976, Atomic Data Nucl. Data Tabl. **18**, 305; 1978, *ibid.* **22**, 371

Howard, W. M., Goriely, S., Rayet, M., & Arnould, M. 1993, Ap. J., **417**, 713

Hurley, K. et al. 1999, Nature (London) **397**, 41

Ignatyuk, A.V., Smirenkin, G.N., & Tishin, A.S. 1975, Yad. Phys. **21** 485 [Sov. J. Nucl. Phys. 29 (1979) 450]

Jeukenne, J.P., Lejeune, A., & Mahaux, C. 1977, Phys. Rev. C **16**, 80

Kaplan, D.L. et al. 2001, ApJ **556**, 399

Kaspi, V.M., Chakrabarty, D., & Steinberger, J. 1999, ApJ, **525**, L33

Kondratyev, V.N. 2001, JAERI-Conf. 2001 - 12, 14

———. 2001a, Abstracts of 2nd Int. Symp. on Advanced Science Research: it Advances in Heavy Element Research (JAERI, Tokai, Japan, Nov. 13 - 15, 2001) P. 60, and J. of Nucl. and Radiochem. Sci. in press

——— . 2002, JAERI-Research 2001-057

——— . 2002a, Phys. Lett. B (submitted)

Kondratyev, V.N., & Di Toro, M. 1996, Phys. Rev. C, 53, 2176

Kondratyev, V.N., & Lutz, H.O. 1998, Phys. Rev. Lett., 81, 4508

———. 1999, Eur. Phys. J. D, 9, 483

Kondratyev, V.N., Maruyama , T., & Chiba, S. 2000, Phys. Rev. Lett., 84, 1086

——— . 1999, JAERI-Research 99-065

——— . 2000a, JAERI -Conf. 2000-011, 99

——— . 2001, ApJ, 546, 1137

——— . 2002, J. Nucl. Sci. Tech. in press

Kouveliotou, C., Dieters, S., Strohmayer, T., van Paradijs, J., Fishman, G.J., Meegan, C.A., Hurley, K., Kommers, J., Smith, I. Frail, D., & Murakami, T. 1998, Nature(London) 393, 235

Kouveliotou, C., Strohmayer, T., Hurl ey, K., van Paradijs, J., Finger, M.H., Dieters, S., Woods, P., Thompson, C., & Duncan, R.C. 1999, ApJ, 510, L115

Kratz, K.-L., Bitouzet, J.-P., Thielemann, F.-K., Möller, P., Pfeiffer, B. 1993, Ap. J. **402**, 216

Kratz, K.-L., Pfeiffer, B., Thielemann, F.-K., 1997, Nucl. Phys. A,

Kratz, K.-L., Thielemann, F.-K., Hillebrandt, W., Möller, P., Harms, V., Truran, J. W. 1988, J. Phys. G **14**, 331

Kratz, K.-L., Thielemann, F.-K., Möller, P., Pfeiffer, B. 1994, in Proc. 8th Int. Symp. on Capture Gamma-Ray Spectroscopy, ed. J. Kern, IOP Bristol, p.724

Lattimer, J. M., Mackie, F., Ravenhall, D. G., & Schramm, D. N. 1977, Ap. J. **213**, 225

Mahaux, C., 1982, Phys. Rev. C **82**, 1848

Mahaux, C., & Weidenmüller, H.A. 1979, Ann. Rev. Part. Nucl. Sci. **29** 1

Mathews, G.J., Bazan, G., Cowan, J.J. 1992, Ap. J. **391**, 719

Mazets, E.P., Golentskii, S.V., Ilinskii, V.N., Aptekar, R.L. & Guryan, Iu.A. 1979, Nature (London) **282**, 587

Meyer, B. S. 1989, Ap. J. **343**, 254

———. 1994, Ann. Rev. Astron. Astrophys. **32**, 153

Meyer, B.S., Mathews, G.J., Howard, W.M., Woosley, S.E., & Hoffman, R.D. 1992, Ap. J. **399**, 656

Meyer, B.S., & Brown, J.S. 1997, ApJ: Supplement Series **112**, 199

Michaud, G. & Fowler, W.A. 1972, ApJ **173**, 157

Möller, P., Nix, J.R., Myers, W.D., & Swiatecki, W.J.1995, At. & Nucl. Data Tables **59**, 185

Nakada, H. & Alhassid, Y. 1997, Phys. Rev. Lett. **79**, 2939

Nilsson, S.G., & Ragnarsson, I. 1990, Shapes and Shells in Nuclear Structure (Cambridge Univ. Press, Cambridge)

Orr, N. A. 1991, Phys. Lett. B **258**, 29

Oyamatsu, K., & Yamada, M. 1994, Nucl. Phys. A578, 181

Ozawa, A. Kobayashi, T. Suzuki, T. Yoshida, K. & Tanihata, I. Phys. Rev. Lett., 2000, **82**, 5493

Pearson, J. M., Nayak, R. C., Goriely, S. 1996, Phys. Lett. B **387**, 455

Pfeiffer, B., Kratz, K.-L., Thielemann, F.-K. 1997, Z. f. Phys. A **357**, 235

Qian, Y.-Z., Woosley, S. E. 1996, Ap. J., 471, 331

Rauscher, T. Thielemann, F.-K., & Kratz, K.-L. 1997, Phys. Rev. C **56**, 1613

Rolfs, C.E., & Rodney, W.S. 1988, Cauldrons in the Cosmos (Chicago Univ. Press, Chicago)

Sneden, C., McWilliam, A., Preston, G. W., Cowan, J. J., Burris, D. I., & Armosky, B. J. 1996, Ap. J. **467**, 819

Sorlin, O. et al. 1993, Phys. Rev. C **47**, 2941

Strutinsky, V.M. 1967, Nucl. Phys. A95, 420

——— . 1968, Nucl. Phys. A122, 1

Surman, R., Engel, J., Bennett, J. R., Meyer, B. S. 1997, Phys. Rev. Lett. **79**, 1809

Surman, R., & Engel, J. 2001, Phys. Rev. C **64**, 035801

Takahashi, K., Witti, J., & Janka, H.-T. 1994, A&A **286**, 857

Terletskii, Ya.P. 1939, Zhurn. Eksp. Teor. Fiz. **9**, 796

Thielemann, F.-K., Arnould, M., & Hillebrandt, W. 1979, A & A. **74**, 175

Thielemann, F.-K., Arnould, M., Truran, J. W. 1987, in *Advances in Nuclear Astrophysics*, ed. E. Vangioni-Flam, Gifsur Yvette, Editions Frontière, p.525

Thielemann, F.-K., Metzinger, J., Klapdor, H.V. 1983, Z. Phys. A **309**, 301

Thielemann, F.-K., Bitouzet, J.-P., Kratz, K.-L., Möller, P., Cowan, J. J., & Truran, J. W. 1993, Phys. Rep. **227**, 269

Thielemann, F.-K., Kratz, K.-L., Pfeiffer, B., Rauscher, T., van Wormer, L., & Wiescher, M. C. 1994, Nucl. Phys. A **570**, 329c

Thompson, C. 2000, ApJ **534**, 915

Thompson, C. & Murray, N. 2001, ApJ **560**, 339

Truran, J.W., Cameron, A.G.W., Gilbert, A. 1966, Can. J. Phys. **44**, 563

Truran, J.W. 1972, Astrophys. Space Sci. **18**, 308

van Leeuwen, J.A. 1921, J. Phys. (Paris) **2**, 361

Varner, R.L. Thompson, W.J., McAbee, T.L. Ludwig, E.J., Clegg, T.B. 1991, Phys. Rep. **201**, 57

Werner, T. R., Sheikh, J. A., Nazarewicz, W., Strayer, M. R., Umar, A. S., Misu, M. 1994, Phys. Lett. B **333**, 303

Woosley, S. E., Hoffman, R. D. 1992, Ap. J. **395**, 202

Woosley, S. E., Wilson, J. R., Mathews, G. J., Hoffman, R. D., Meyer, B. S. 1994, Ap. J. **433**, 229

Zuker, A.P. 2001, Phys. Rev. C**64**, 021303

This plano tables was prepared with the AAS LaTeX macros v4.0.

国際単位系(SI)と換算表

表1　SI基本単位および補助単位

量	名称	記号
長さ	メートル	m
質量	キログラム	kg
時間	秒	s
電流	アンペア	A
熱力学温度	ケルビン	K
物質量	モル	mol
光度	カンデラ	cd
平面角	ラジアン	rad
立体角	ステラジアン	sr

表2　SIと併用される単位

名称	記号
分，時，日	min，h，d
度，分，秒	°，′，″
リットル	l，L
トン	t
電子ボルト	eV
原子質量単位	u

1 eV = 1.60218 × 10^{-19} J

1 u = 1.66054 × 10^{-27} kg

表3　固有の名称をもつSI組立単位

量	名称	記号	他のSI単位による表現
周波数	ヘルツ	Hz	s^{-1}
力	ニュートン	N	$m\cdot kg/s^2$
圧力，応力	パスカル	Pa	N/m^2
エネルギー，仕事，熱量	ジュール	J	N·m
工率，放射束	ワット	W	J/s
電気量，電荷	クーロン	C	A·s
電位，電圧，起電力	ボルト	V	W/A
静電容量	ファラド	F	C/V
電気抵抗	オーム	Ω	V/A
コンダクタンス	ジーメンス	S	A/V
磁束	ウェーバ	Wb	V·s
磁束密度	テスラ	T	Wb/m^2
インダクタンス	ヘンリー	H	Wb/A
セルシウス温度	セルシウス度	℃	
光束	ルーメン	lm	cd·sr
照度	ルクス	lx	lm/m^2
放射能	ベクレル	Bq	s^{-1}
吸収線量	グレイ	Gy	J/kg
線量当量	シーベルト	Sv	J/kg

表4　SIと共に暫定的に維持される単位

名称	記号
オングストローム	Å
バーン	b
バール	bar
ガル	Gal
キュリー	Ci
レントゲン	R
ラド	rad
レム	rem

1 Å = 0.1 nm = 10^{-10} m

1 b = 100 fm^2 = 10^{-28} m^2

1 bar = 0.1 MPa = 10^5 Pa

1 Gal = 1 cm/s^2 = 10^{-2} m/s^2

1 Ci = 3.7 × 10^{10} Bq

1 R = 2.58 × 10^{-4} C/kg

1 rad = 1 cGy = 10^{-2} Gy

1 rem = 1 cSv = 10^{-2} Sv

表5　SI接頭語

倍数	接頭語	記号
10^{18}	エクサ	E
10^{15}	ペタ	P
10^{12}	テラ	T
10^{9}	ギガ	G
10^{6}	メガ	M
10^{3}	キロ	k
10^{2}	ヘクト	h
10^{1}	デカ	da
10^{-1}	デシ	d
10^{-2}	センチ	c
10^{-3}	ミリ	m
10^{-6}	マイクロ	μ
10^{-9}	ナノ	n
10^{-12}	ピコ	p
10^{-15}	フェムト	f
10^{-18}	アト	a

（注）

1. 表1－5は「国際単位系」第5版，国際度量衡局 1985年刊行による。ただし，1 eVおよび1 uの値はCODATAの1986年推奨値によった。
2. 表4には海里，ノット，アール，ヘクタールも含まれているが日常の単位なのでここでは省略した。
3. barは，JISでは流体の圧力を表わす場合に限り表2のカテゴリーに分類されている。
4. EC閣僚理事会指令ではbar，barnおよび「血圧の単位」mmHgを表2のカテゴリーに入れている。

換算表

力	N(=10^5 dyn)	kgf	lbf
	1	0.101972	0.224809
	9.80665	1	2.20462
	4.44822	0.453592	1

粘度　1 Pa·s(N·s/m^2) = 10 P(ポアズ)(g/(cm·s))

動粘度　1 m^2/s = 10^4 St(ストークス)(cm^2/s)

圧力	MPa(=10 bar)	kgf/cm^2	atm	mmHg(Torr)	lbf/in^2(psi)
	1	10.1972	9.86923	7.50062 × 10^3	145.038
	0.0980665	1	0.967841	735.559	14.2233
	0.101325	1.03323	1	760	14.6959
	1.33322 × 10^{-4}	1.35951 × 10^{-3}	1.31579 × 10^{-3}	1	1.93368 × 10^{-2}
	6.89476 × 10^{-3}	7.03070 × 10^{-2}	6.80460 × 10^{-2}	51.7149	1

エネルギー・仕事・熱量	J(=10^7 erg)	kgf·m	kW·h	cal(計量法)	Btu	ft·lbf	eV
	1	0.101972	2.77778 × 10^{-7}	0.238889	9.47813 × 10^{-4}	0.737562	6.24150 × 10^{18}
	9.80665	1	2.72407 × 10^{-6}	2.34270	9.29487 × 10^{-3}	7.23301	6.12082 × 10^{19}
	3.6 × 10^6	3.67098 × 10^5	1	8.59999 × 10^5	3412.13	2.65522 × 10^6	2.24694 × 10^{25}
	4.18605	0.426858	1.16279 × 10^{-6}	1	3.96759 × 10^{-3}	3.08747	2.61272 × 10^{19}
	1055.06	107.586	2.93072 × 10^{-4}	252.042	1	778.172	6.58515 × 10^{21}
	1.35582	0.138255	3.76616 × 10^{-7}	0.323890	1.28506 × 10^{-3}	1	8.46233 × 10^{18}
	1.60218 × 10^{-19}	1.63377 × 10^{-20}	4.45050 × 10^{-26}	3.82743 × 10^{-20}	1.51857 × 10^{-22}	1.18171 × 10^{-19}	1

1 cal = 4.18605 J(計量法)

= 4.184 J　(熱化学)

= 4.1855 J　(15 °C)

= 4.1868 J(国際蒸気表)

仕事率　1 PS(仏馬力)

= 75 kgf·m/s

= 735.499 W

放射能	Bq	Ci
	1	2.70270 × 10^{-11}
	3.7 × 10^{10}	1

吸収線量	Gy	rad
	1	100
	0.01	1

照射線量	C/kg	R
	1	3876
	2.58 × 10^{-4}	1

線量当量	Sv	rem
	1	100
	0.01	1

（86年12月26日現在）

Nuclear Reactions in Ultra-magnetized Supernovae